# Greater India Basin hypothesis and a two-stage Cenozoic collision between India and Asia

Douwe J. J. van Hinsbergen[a,b,1], Peter C. Lippert[c,d], Guillaume Dupont-Nivet[e,f,g], Nadine McQuarrie[h], Pavel V. Doubrovine[a,b], Wim Spakman[i], and Trond H. Torsvik[a,b,j,k]

[a]Physics of Geological Processes, University of Oslo, Sem Sælands vei 24, NO-0316 Oslo, Norway; [b]Center for Advanced Study, Norwegian Academy of Science and Letters, Drammensveien 78, 0271 Oslo, Norway; [c]Department of Geosciences, University of Arizona, Tucson, AZ 85721; [d]Department of Earth and Planetary Sciences, University of California, Santa Cruz, CA 95064; [e]Géosciences Rennes, Unité Mixte de Recherche 6118, Université de Rennes 1, Campus de Beaulieu, 35042 Rennes Cedex, France; [f]Paleomagnetic Laboratory Fort Hoofddijk, Department of Earth Sciences, University of Utrecht, Budapestlaan 17, 3584 CD, Utrecht, The Netherlands; [g]Key Laboratory of Orogenic Belts and Crustal Evolution, Ministry of Education, Peking University, Beijing 100871, China; [h]Department of Geology and Planetary Science, University of Pittsburgh, Pittsburgh, PA 15260; [i]Department of Earth Sciences, University of Utrecht, Budapestlaan 4, 3584 CD, Utrecht, The Netherlands; [j]Center for Geodynamics, Geological Survey of Norway, Leiv Eirikssons vei 39, 7491 Trondheim, Norway; and [k]School of Geosciences, University of the Witwatersrand, WITS 2050, Johannesburg, South Africa

Edited by B. Clark Burchfiel, Massachusetts Institute of Technology, Cambridge, MA, and approved March 29, 2012 (received for review October 19, 2011)

**Cenozoic convergence between the Indian and Asian plates produced the archetypical continental collision zone comprising the Himalaya mountain belt and the Tibetan Plateau. How and where India–Asia convergence was accommodated after collision at or before 52 Ma remains a long-standing controversy. Since 52 Ma, the two plates have converged up to 3,600 ± 35 km, yet the upper crustal shortening documented from the geological record of Asia and the Himalaya is up to approximately 2,350-km less. Here we show that the discrepancy between the convergence and the shortening can be explained by subduction of highly extended continental and oceanic Indian lithosphere within the Himalaya between approximately 50 and 25 Ma. Paleomagnetic data show that this extended continental and oceanic "Greater India" promontory resulted from 2,675 ± 700 km of North–South extension between 120 and 70 Ma, accommodated between the Tibetan Himalaya and cratonic India. We suggest that the approximately 50 Ma "India"–Asia collision was a collision of a Tibetan-Himalayan microcontinent with Asia, followed by subduction of the largely oceanic Greater India Basin along a subduction zone at the location of the Greater Himalaya. The "hard" India–Asia collision with thicker and contiguous Indian continental lithosphere occurred around 25–20 Ma. This hard collision is coincident with far-field deformation in central Asia and rapid exhumation of Greater Himalaya crystalline rocks, and may be linked to intensification of the Asian monsoon system. This two-stage collision between India and Asia is also reflected in the deep mantle remnants of subduction imaged with seismic tomography.**

continent–continent collision | mantle tomography | plate reconstructions | Cretaceous

The present geological boundary between India and Asia is marked by the Indus–Yarlung suture zone, which contains deformed remnants of the ancient Neotethys Ocean (1, 2) (Fig. 1). North of the Indus–Yarlung suture is the southernmost continental fragment of Asia, the Lhasa block. South of the suture lies the Himalaya, composed of (meta)sedimentary rocks that were scraped off now-subducted Indian continental crust and mantle lithosphere and thrust southward over India during collision. The highest structural unit of the Himalaya is overlain by fragments of oceanic lithosphere (ophiolites).

We apply the common term Greater India to refer to the part of the Indian plate that has been subducted underneath Tibet since the onset of Cenozoic continental collision. A 52 Ma minimum age of collision between northernmost Greater India and the Lhasa block is constrained by 52 Ma sedimentary rocks in the northern, "Tibetan" Himalaya that include detritus from the Lhasa block (3). This collision age is consistent with independent paleomagnetic evidence for overlapping paleolatitudes for the Tibetan Himalaya and the Lhasa blocks at 48.6 ± 6.2 Ma (Fig. 2; *SI Text*) as well as with an abrupt decrease in India–Asia convergence rates beginning at 55–50 Ma, as demonstrated by India–Asia plate circuits (e.g., ref. 4). Structural (5) and stratigraphic (6) data show that ophiolites were emplaced over the Tibetan Himalaya in the latest Cretaceous (approximately 70–65 Ma), well before the Tibetan Himalaya–Lhasa collision. Paleomagnetic data suggest that these ophiolites formed at equatorial paleolatitudes (7).

Motion between continents that border the modern oceans is quantified through time using plate reconstructions based on marine magnetic anomalies. The Eurasia-North America-Africa-India plate circuit demonstrates 2,860 ± 30 and 3,600 ± 35 km of post-52 Ma India–Asia convergence for the western and eastern Himalayan syntaxes, respectively (4). It has long been recognized that the amount of upper crustal shortening since 52 Ma reconstructed from the geology of the Himalaya and Asia accounts for only approximately 30–50% of this total convergence (8) (Fig. 1). Previously proposed solutions for this "shortening deficit" include major unrecognized shortening in Siberia (8, 9), a >1,000-km eastward extrusion of Indochina from an original position within Tibet that would lead to >2,000 km of Cenozoic intra-Asian shortening (10–12), or a much younger Tibetan Himalaya–Lhasa collision (13). However, geologically reconstructed shortening of approximately 1,050–600 km (from west to east) within and north of the Pamir and the Tibetan plateau without invoking major Indochina extrusion (14) is consistent with 1,100 ± 500 km of paleomagnetically constrained convergence between the Indus–Yarlung suture and Eurasia since approximately 50 Ma (15). The excess convergence should therefore mostly have been accommodated in the Himalaya, to the south of the Indus–Yarlung suture.

The Himalaya consists of upper continental crust that was decoupled from now-subducted Greater India (1, 2), which is generally considered to have formed the contiguous margin of northern India (2, 16–18). The Himalaya is divided into three tectonostratigraphic zones (Fig. 1). From north to south, these include the non- to low-metamorphic grade sedimentary rocks of the Tibetan Himalaya, separated by the South Tibetan detachment from the igneous and high-grade metamorphic Greater Himalaya, which overlies the low-grade, internally thrusted Lesser Himalaya along the Main Central thrust (1, 2) (Fig. 1).

Author contributions: D.J.J.v.H. designed research; D.J.J.v.H., P.C.L., G.D.-N., N.M., P.V.D., W.S., and T.H.T. performed research; D.J.J.v.H. and P.C.L. analyzed data; and D.J.J.v.H., P.C.L., G.D.-N., and N.M. wrote the paper.

The authors declare no conflict of interest.

This article is a PNAS Direct Submission.

[1]To whom correspondence should be addressed. E-mail: d.v.hinsbergen@fys.uio.no.

This article contains supporting information online at www.pnas.org/lookup/suppl/doi:10.1073/pnas.1117262109/-/DCSupplemental.

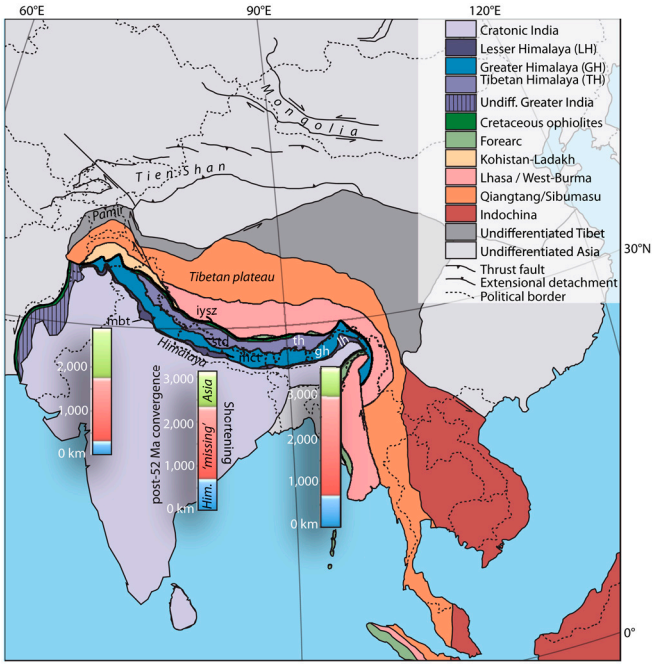


**Fig. 1.** Tectonic map of the India–Asia collision zone. Bars represent the amount of post-50 Ma India–Asia convergence, and the amount of intra-Asian (14), Himalayan (19, 20), and missing shortening along the collision zone. We calculated the Himalayan shortening deficit using a reconstruction of Asian deformation (14) embedded in global plate circuits (4, 34). Our maximum estimate of undocumented convergence uses (*i*) plate convergence estimates since 50 Ma, 3,600 ± 35 km for the eastern Himalayan syntaxis (4); (*ii*) approximately 600 km of shortening reconstructed in eastern Tibet since 50 Ma (14); and (*iii*) up to 650 km of shortening reconstructed from the eastern Himalaya (51), resulting in a 2,350 km deficit. Since approximately 25–20 Ma, the total amount of plate convergence is up to 1,300–1,000 km in the eastern Himalaya (4). Shortening since approximately 25 Ma in the Himalaya, along the main central thrust (MCT) and in the Lesser Himalaya (LH), is approximately 400–700 km (20), and in Tibet, approximately 200–300 km (14), leaving a modest shortening deficit of several hundreds of kilometers. We ascribe this deficit to uncertainties in the Tibet reconstruction, uncertainties in the timing of Tibetan Himalaya (TH) shortening, and the fact that balanced cross-sections provide minimum estimates. STD, South Tibetan Detachment; IYSZ, Indus–Yarlung Suture Zone; MBT, main boundary thrust.

Composite balanced cross-sections across the Himalaya documented approximately 500–900 km of shortening (19, 20). These estimates are the sum of (*i*) shortening in the Tibetan Himalaya (since the Paleogene); (*ii*) the amount of overlap between the Greater Himalaya and the Lesser Himalaya along the Main Central thrust that was largely established between approximately 25–20 and 15–10 Ma; and (*iii*) the amount of shortening within the Lesser Himalaya since approximately 15–10 Ma (2, 19, 20). The main uncertainty in the Himalayan shortening estimates are associated with the Greater Himalaya. Intense Miocene deformation has effectively overprinted any older structures in the Greater Himalaya, but well-dated prograde mineral growth and magmatism in the Greater Himalaya shows evidence for burial and heating between 45 and 25 Ma (21–23). The amount of shortening accommodated within or below the Greater Himalaya prior to the Miocene therefore remains geologically unconstrained, but could be considerable. Detrital zircon studies of the Lesser, Greater, and Tibetan Himalaya suggest that their Neoproterozoic to lower Paleozoic (Cambrian-Ordovician) stratigraphies are similar (16, 24–26), suggesting that the net effect of post-Ordovician tectonics within the Himalaya was limited to perhaps several hundreds of kilometers of shortening.

The amount of India–Asia convergence since 52 Ma (up to 3,600 ± 35 km, ref. 4) exceeds the estimated total crustal shortening within Asia and the Himalaya by up to 2,350 km (14, 19, 20) (Fig. 1). In this paper, we will consider several possible explanations of the observed discrepancy and propose a tectonic scenario that can reconcile the disparate estimates and identify the structure(s) that accommodated the 'missing' convergence.

## Size of Greater India Through Time

The only available technique to quantify past motions between continental blocks that are not connected through a passive margin to oceanic basins is paleomagnetism. A wealth of paleomagnetic data from the Ordovician, Triassic, and lower Cretaceous rocks of the Tibetan Himalaya consistently demonstrates minor net North–South (N-S) motion of the Tibetan Himalaya relative to India since these times (*SI Text*). The youngest rocks that demonstrate a relatively small Greater India are approximately 120 Mya old and show a net convergence between India and the Tibetan Himalaya of 2.1 ± 5.5°, or 233 ± 877 km (Fig. 2). After adding the modern width of Greater India (i.e., the Himalaya, approximately 250 km N-S), these data suggest that Greater India in early Cretaceous time was not larger than approximately 900 km (*SI Text*). This conclusion is consistent with pre-Cretaceous Gondwana plate reconstructions (17, 27) as well as with the notion that the Paleozoic and older stratigraphies of the Himalayan zones are correlative, suggesting that during their deposition Greater India formed a contiguous continental margin (16, 24–26). By assuming that Greater India remained only several hundreds of kilometers wide until collision with Asia, Aitchison et al. (13, 28) demonstrated that the leading edge of Greater India would have passed the equator approximately 55 Ma ago, and suggested that the 55–50 Ma collision record (what is widely regarded as the Tibetan Himalaya–Asia collision) resulted from just the obduction of ophiolites onto the leading, Tibetan-Himalayan edge of Greater India. By also assuming negligible Cenozoic intra-Asian shortening, their model proposed that the India–Asia collision occurred at approximately 34 Ma. Paleomagnetic evidence from upper Cretaceous (approximately 68 Ma) and Paleocene (approximately 59 Ma) rocks from the Tibetan Himalaya (29–31) and cratonic India, however, demonstrate that during the late Cretaceous to Paleocene, the Tibetan Himalaya was separated by 22.0 ± 3.0° of latitude (2,442 ± 333 km N-S) from India (Fig. 2). These paleomagnetic data pass both fold and reversal paleomagnetic field tests at high confidence (*SI Text*), demonstrating their prefolding, primary magnetic acquisition. This much larger size of Greater India at the time of collision than during the early Cretaceous results in a paleomagnetically determined collision age of 48.6 ± 6.2 Ma (Fig. 2; *SI Text*), consistent with the 52 Ma age of first arrival of Lhasa-derived sediments in the Tibetan Himalaya (3). This large dimension of Greater India is also consistent with the position of the southern Asian margin at the time of collision based on restoration of intra-Asian deformation (14). Therefore, paleomagnetic data show that between 118 and 68 Ma, Greater India became extended and the Tibetan Himalaya drifted 24.1 ± 6.3° (2,675 ± 699 km N-S) northward relative to cratonic India (Fig. 2), followed by convergence of a similar magnitude after collision.

## Cretaceous Greater Indian N-S Extension

Cretaceous extension within Greater India has previously been inferred from sedimentary facies changes in the Tibetan Himalaya (17, 18) and from lower Cretaceous (140–100 Ma) alkali-basaltic volcaniclastic sediments with a geochemistry interpreted to record intracontinental rifting (32, 33). The 2,675 ± 700 km of N-S extension between 118 and 68 Ma, inferred from paleomagnetic data (Fig. 2), requires minimum extension rates of 40–67 mm/y. Such rates are typical for midoceanic ridges (predrift continental extension rates rarely exceed 20 mm/y, ref. 34), and the magnitude of extension is an order of magnitude larger than that of typical extended continental margins (34). Thus, at least one oceanic basin—the Greater India Basin(s) (GIB)—must have formed between the Tibetan Himalaya and cratonic

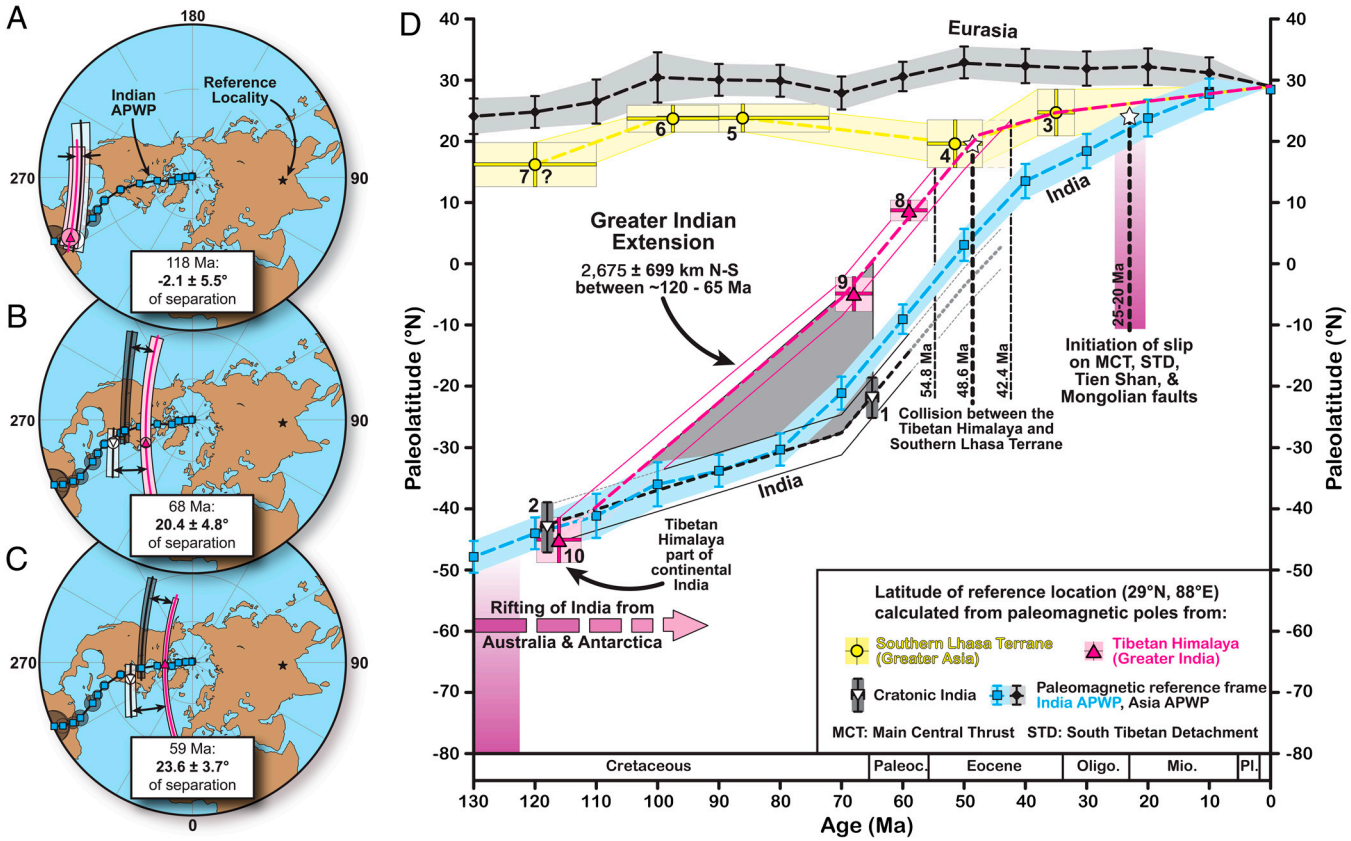


**Fig. 2.** Paleolatitude evolution of India, Greater India, Greater Asia, and Asia. (*A*) Paleomagnetic poles for the Tibetan Himalaya (magneta upright triangle) and cratonic India (white downward triangle) at 118 Ma, compared to the Indian apparent polar wander path (APWP) (blue squares), indicating that the net N-S drift of the Tibetan Himalaya relative to India since 118 Ma was negligible; Greater India was not larger than approximately 900 km (*SI Text*). Ninety-five percent confidence intervals of the pole positions are also shown. (*B* and *C*) Same as *A*, but at 68 and 59 Ma, respectively, indicating 2,675 ± 699 km of northward drift of the Tibetan Himalaya relative to continental India compared to their 118 Ma position. (*D*) Paleolatitudes of a reference site (29°N, 88°E) located on the present-day position of the Indus–Yarlung Suture Zone in Eurasian, Greater Asian, Tibetan-Himalayan, and Indian reference frames. Numbers correspond to paleomagnetic poles described and listed in the *SI Text*. Pl, Pliocene; Mio, Miocene; Oligo, Oligocene; Paleoc., Paleocene; MCT, main central thrust; STD, South Tibetan detachment. Age uncertainties are based on the age of the units determined from either radiometric dates or geologic stages (52, 53), and latitude uncertainties are calculated from the corresponding poles at the 95% confidence level. Question mark next to estimate 7 indicates that this pole may insufficiently average paleosecular variation. See *SI Text* for details.

India, separating a microcontinent from cratonic India (Fig. 3). The paleogeography of extended Greater India may have consisted of one or more deep basins alternating with (stretched) continental fragments, similar to Mediterranean paleogeography (35). The Cretaceous extension that would have opened the GIB (2,675 ± 700 km) encompasses the approximately 2,350 km of plate convergence that remains undocumented in the geological record of the Himalaya (Fig. 1). Numerical models demonstrate that continental lithosphere can subduct if its buoyant upper crust becomes decoupled from the subducting continent, but denser oceanic or thinned continental lithosphere can subduct without accretion (36). These modeling results are consistent with the observation that many convergent margins with oceanic subduction are nonaccreting (37). If 2,675 ± 700 km of extension created up to approximately 2,350 km of oceanic crust and highly extended continental margins in the GIB, subduction of that crust thus provides a straightforward explanation for the discrepancy between convergence and shortening.

## Subduction History and Mantle Tomography

Subduction of the GIB following the approximately 50 Ma Tibetan Himalaya–Lhasa collision is consistent with seismic tomographic images of the mantle beneath India and Tibet. These images reveal three prominent velocity anomalies that have been interpreted as subducted Indian plate lithosphere (38–40) (Fig. 4). The deepest anomaly, at approximately 900 km and greater depth, is generally considered subducted Neotethyan oceanic lithosphere, detached sometime after the Tibetan Himalaya–Lhasa collision (38–40). A shallower anomaly between approximately 400- and 850-km depth would hence be Cenozoic in age (38–40); it projects directly below the reconstructed position of the Tibetan Himalaya between 50 and 25 Ma (Fig. 4). A third conspicuous body imaged horizontally below Tibet over a distance of approximately 500 km from the Himalayan front represents Indian continental lithosphere that has underthrust Asia since the last phase of slab break-off (39, 41). Taking Asian shortening (14) into account, this horizontal body represents the last 10–15 Ma of India–Asia convergence.

Seismic tomographic images also show anomalies in the lower mantle at equatorial latitudes (Fig. 4*A*), generally interpreted as a result of Cretaceous intraoceanic subduction (40, 42). Aitchison et al. (28) suggested that this anomaly resulted from intraoceanic subduction that terminated with ophiolite obduction onto the leading edge of Greater India. We agree that this anomaly represents the relict of an intraoceanic subduction zone, but we note that the much larger size of Greater India in late Cretaceous time shown by paleomagnetic data (Fig. 2) positions the northern margin of the Tibetan Himalaya above this equatorial lower mantle anomaly around 70 Ma, not 55 Ma (Figs. 3 and 4). This reconstruction is consistent with structural and stratigraphic evidence for ophiolite obduction onto the Tibetan Himalaya at approximately 70 Ma (5, 6).

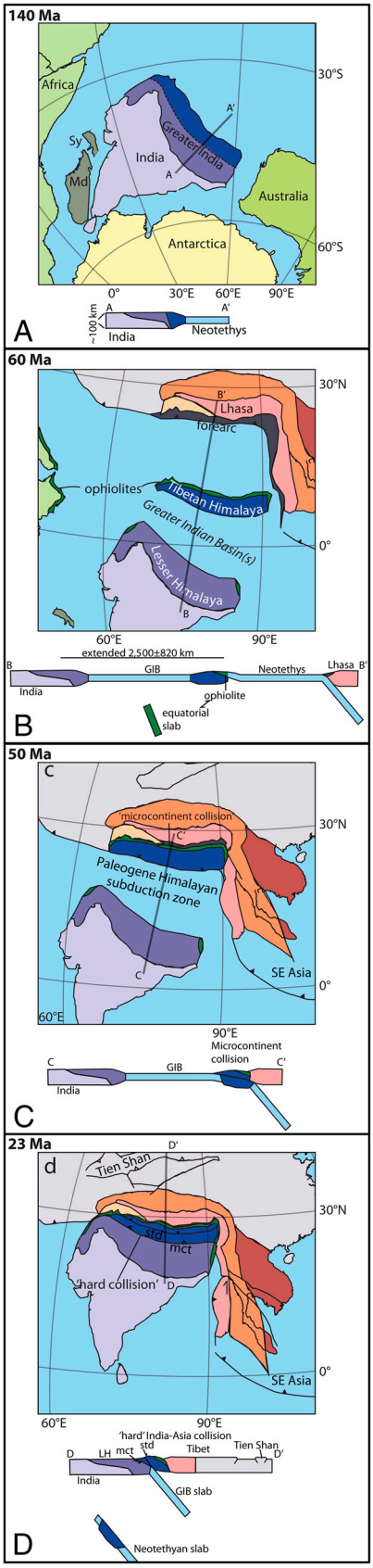


**Fig. 3.** Plate reconstruction of the India–Asia collision (4, 54). A small Greater India (*A*) was extended in the Cretaceous (*B*), leading to a "soft" collision and ongoing subduction around 50 Ma (*C*) and a "hard" collision with thick, continuous Indian lithosphere between 25 and 20 Ma (*D*). MCT, main central thrust; Md, madagascar; STD, South Tibetan detachment; Sy, Seychelles.

## Location of a Paleogene Subduction Zone Within the Himalaya

The collision between the Tibetan Himalayan microcontinent and Asia at approximately 50 Ma, and the subsequent closure of the Greater India Basin south of this microcontinent, requires a Paleogene to Miocene subduction zone south of (i.e., structurally below) the Tibetan Himalaya. The location of this subduction zone must be located somewhere within the modern Himalayan thrust belt, and therefore has implications for the interpretation of existing geological evidence on the contemporaneous evolution of the Himalaya (Fig. 3).

Since the onset of thrusting of the Greater Himalaya over the Lesser Himalaya along the Main Central thrust approximately 25–20 Ma ago, cumulative shortening in the Himalaya (19, 20) and Asia (14) is close to contemporaneous India–Asia convergence (4) (approximately 1,000 km). The continental clastic rocks of the Lesser Himalaya demonstrate continuous subduction of continental lithosphere and accretion of its upper crust to the Himalaya in this time interval. Thus, the discrepancy between predicted convergence and measured shortening is largely concentrated between 50 and approximately 25–20 Ma. Because the Tibetan Himalaya collided with Asia at or before approximately 50 Ma, and the deformation of the Lesser Himalaya is Miocene in age (43), 50–25 Ma convergence must have been accommodated structurally below (i.e., south of) the Tibetan, but above (i.e., north of) the Lesser Himalaya. As mentioned before, the total displacement along the Main Central thrust, as well as convergence accommodated within the Greater Himalaya, remains unknown due to severe Miocene deformation; however, well-dated prograde mineral growth and magmatism (21–23, 44) in the Greater Himalaya shows evidence for burial and heating between 45 and 25 Ma. If Cretaceous extension opened a single Greater Indian Ocean separating a microcontinent from India (Fig. 3), then these Paleogene metamorphic ages would suggest that the Greater and Tibetan Himalaya both belonged to a single microcontinent that collided with and accreted to Asia around 50 Ma. During the 50–25 Ma subduction of the Indian Plate (i.e., the GIB), the Greater and Tibetan Himalaya would then have thickened and metamorphosed as part of the compressed overriding plate (i.e., together with the Tibetan plateau to the north). Subduction—without accretion—would have been concentrated along a precursor of the Main Central thrust. If the GIB had a more complex paleogeography, then the Greater Himalaya could contain a ductile thrust stack (duplex) of deep marine rocks underplated and metamorphosed below the Tibetan Himalaya throughout the Paleogene. Pre-25-Ma prograde metamorphic ages in the Greater Himalaya vary considerably, from 45 Ma migmatitic rocks in gneiss domes in the Tibetan Himalaya (21) to 25 Ma eclogites in Nepal (23); these ages may represent the different times at which Greater Himalayan rocks were structurally buried in the duplex. In any case, the GIB suture lies either structurally within or below the Greater Himalaya.

## Microcontinent–Continent Collision (50 Ma) and India–Asia Collision (25–20 Ma)

In our model, the approximately 50 Ma India–Asia collision epresents collision of an extended microcontinental fragment (that contained the rocks now found in the Tibetan Himalaya) and continental Asia. This collision led to orogeny (14, 45), but was followed by ongoing oceanic subduction of the GIB. The hard continent–continent collision followed approximately 25 Ma later with the arrival of much less extended, contiguous continental Indian lithosphere to the collision zone, leading to increased coupling at the plate contact (46). Such increased coupling is consistent with (*i*) the similarity between shortening and convergence since 25–20 Ma; (*ii*) the onset of Greater Himalayan extrusion along the South Tibetan detachment and Main Central thrust (2); and (*iii*) the simultaneous and sudden onset of far-field

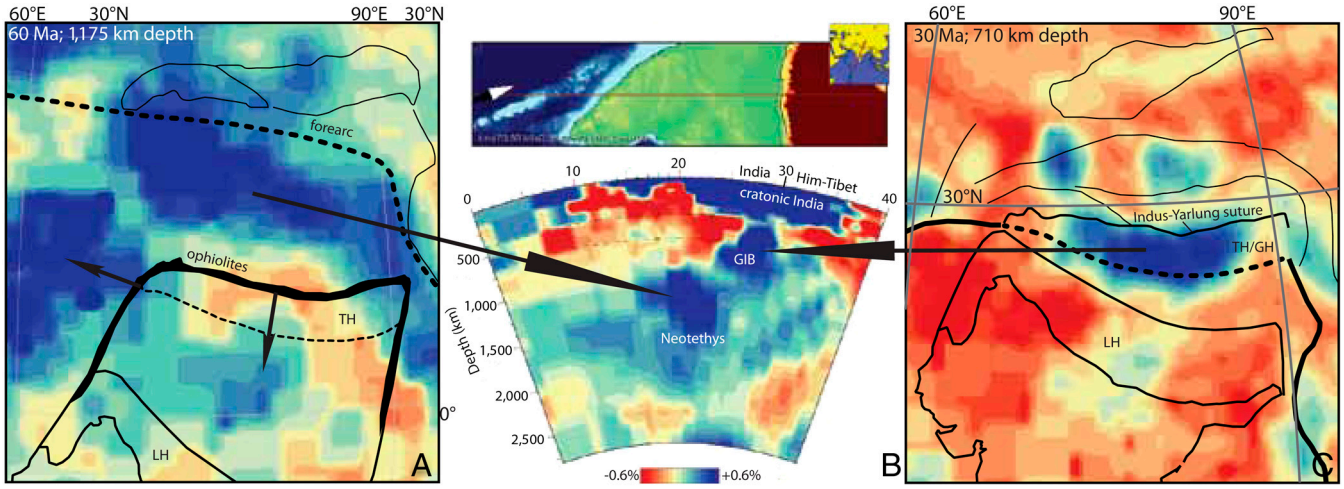


**Fig. 4.** Seismic tomographic images of subducted slabs compared to India–Asia restorations. (*A* and *C*) Sixty and 30 Ma plate reconstructions of the India–Asia collision zone in a moving hotspot reference frame (54) projected above seismic tomographic images, derived from the UU-P07 model (55), at 1,175 (0.6% contours) and 710 km (1% contours) depth, respectively, with previously identified intraoceanic subduction zones (40, 42). (*B*) Vertical cross-section (0.6% contours) of the mantle below the India–Asia collision zone indicating the three major Indian plate mantle anomalies. TH, Tibetan Himalaya; LH, Lesser Himalaya; GH, Greater Himalaya.

deformation into Central Asia (14) (e.g., deforming and uplifting the Tien Shan, ref. 47) (Fig. 1). Comparison of our plate and deformation reconstructions with seismic tomography suggests that this latter collision was followed by slab break-off at approximately 15–10 Ma and horizontal underthrusting of India below Tibet thereafter. The onset of this last phase of India–Asia collision is contemporaneous with a period of outward growth and extension of the Tibetan plateau (10, 12, 48).

The recognition of major Cretaceous extension in India and a multistage India–Asia collision history no longer requires models invoking major continental extrusion from Tibet predicting >2,000 km of Cenozoic intra-Asian convergence (10–12), but is consistent with kinematic and paleomagnetic reconstructions showing <1,000 km of intra-Asian shortening (8, 14, 15, 49). Our model does not require younger initial collision ages (13) and is in line with geological data from the Indus–Yarlung suture zone (3), suggesting an approximately 50 Ma Tibetan Himalaya–Asia collision. It identifies the Greater Himalaya as the exhumed mid- to lower-continental crust that resided directly above a subduction zone from approximately 50 to 25 Ma. Finally, the hard collision was followed by a substantial increase in erosion rates within the Himalayan system, which may reflect a more virgorous South Asian monsoon (50), highlighting another potential link between geodynamic processes forming the Tibetan-Himalayan mountain belt and climate evolution.

**ACKNOWLEDGMENTS.** Paul Kapp, Pete DeCelles, Douwe van der Meer, and Rob van der Voo are thanked for discussion and comments on previous versions of this manuscript. D.J.J.v.H. and T.H.T. acknowledge financial support from Statoil (SPlates Model Project). D.J.J.v.H., P.V.D., and T.H.T. were supported by the Center for Advanced Study of the Norwegian Academy of Science and Letters. T.H.T., P.V.D., and W.S. acknowledge support through the TOPO-Europe TOPO-4D program. Reasearch of W.S. was carried out in context of the Netherlands Research School of Integrated Solid Earth Sciences. G.D.-N. acknowledges support from the Dutch Netherlands Organization for Scientific Research, the French Centre National de la Recherche Scientifique, and the Chinese National Science Foundation. N.M. acknowledges National Science Foundation Grant EAR 0738522. P.C.L. acknowledges National Science Foundation Grant EAR 1008527. D.J.J.v.H. thanks the Carnegie Institution for Science in Washington, DC for their hospitality.

1. Gansser A (1964) *The Geology of the Himalayas* (Wiley Interscience, New York).
2. Hodges KV (2000) Tectonics of the Himalaya and southern Tibet from two perspectives. *Geol Soc Am Bull* 112:324–350.
3. Najman Y, et al. (2010) The timing of India–Asia collision: Geological, biostratigraphic and palaeomagnetic constraints. *J Geophys Res* 115:B12416.
4. van Hinsbergen DJJ, Steinberger B, Doubrovine PV, Gassmöller R (2011) Acceleration and deceleration of India–Asia convergence since the Cretaceous: Roles of mantle plumes and continental collision. *J Geophys Res* 116:B06101.
5. Searle MP, Treloar PJ (2010) Was Late Cretaceous—Palaeocene obduction of ophiolite complexes the primary cause of crustal thickening and regional metamorphism in the Pakistan Himalaya? *The Evolving Continents: Understanding Processes of Continental Growth*, eds TM Kusky, MG Zhai, and W Xiao (Geological Society, London), Special Publication, Vol 338, pp 345–359.
6. Cai F, Ding L, Yue Y (2011) Provenance analysis of upper Cretaceous strata in the Tethys Himalaya, southern Tibet: Implications for timing of India–Asia collision. *Earth Planet Sci Lett* 305:195–206.
7. Abrajevitch AV, et al. (2005) Neotethys and the India–Asia collision: Insights from a palaeomagnetic study of the Dazhuqu ophiolite, southern Tibet. *Earth Planet Sci Lett* 233:87–102.
8. Dewey JF, Shackleton RM, Chang C, Sun Y (1988) The tectonic evolution of the Tibetan Plateau. *Philos Trans R Soc A Math Phys Eng Sci* 327:379–413.
9. Guillot S, et al. (2003) Reconstructing the total shortening history of the NW Himalaya. *Geochem Geophys Geosyst* 4:1064.
10. Royden LH, Burchfiel BC, Van der Hilst RD (2008) The geological evolution of the Tibetan Plateau. *Science* 321:1054–1058.
11. Replumaz A, Tapponnier P (2003) Reconstruction of the deformed collision zone Between India and Asia by backward motion of lithospheric blocks. *J Geophys Res* 108:2285.
12. Tapponnier P, et al. (2001) Oblique stepwise rise and growth of the Tibet Plateau. *Science* 294:1671–1677.
13. Aitchison JC, Ali JR, Davis AM (2007) When and where did India and Asia collide? *J Geophys Res* 112:B05423.
14. van Hinsbergen DJJ, et al. (2011) Restoration of Cenozoic deformation in Asia, and the size of Greater India. *Tectonics* 30:TC5003.
15. Dupont-Nivet G, van Hinsbergen DJJ, Torsvik TH (2010) Persistently shallow paleomagnetic inclinations in Asia: Tectonic implications for the Indo-Asia collision. *Tectonics* 29:TC5016.
16. Myrow PM, et al. (2003) Integrated tectonostratigraphic analysis of the Himalaya and implications for its tectonic reconstruction. *Earth Planet Sci Lett* 212:433–441.
17. Garzanti E (1999) Stratigraphy and sedimentary history of the Nepal Tethys Himalaya passive margin. *J Asian Earth Sci* 17:805–827.
18. Gaetani M, Garzanti E (1991) Multicyclic history of the northern India continental margin (northwestern Himalaya). *AAPG Bull* 75:1427–1446.
19. DeCelles PG, Robinson DM, Zandt G (2002) Implications of shortening in the Himalayan fold-thrust belt for uplift of the Tibetan Plateau. *Tectonics* 21:TC1062.
20. Long SP, McQuarrie N, Tobgay T, Grujic D (2011) Geometry and crustal shortening of the Himalayan fold-thrust belt, eastern and central Bhutan. *Geol Soc Am Bull* 123:1427–1447.
21. Pullen A, Kapp P, DeCelles PC, Gehrels GE, Ding L (2011) Cenozoic anatexis and exhumation of Tethyan Sequence rocks in the Xiao Gurla Range, Southwest Tibet. *Tectonophysics* 501:28–40.
22. Lee J, Whitehouse MJ (2007) Onset of mid-crustal extensional flow in southern Tibet: Evidence from U/Pb zircon ages. *Geology* 35:45–48.
23. Corrie SL, Kohn MJ, Vervoort JD (2010) Young eclogite from the Greater Himalayan Sequence, Arun Valley, eastern Nepal: P-T-t path and tectonic implications. *Earth Planet Sci Lett* 289:406–416.
24. Long S, et al. (2011) Tectonostratigraphy of the Lesser Himalaya of Bhutan: Implications for the along-strike stratigraphic continuity of the northern Indian margin. *Geol Soc Am Bull* 123:1258–1274.

25. Yin A (2006) Cenozoic tectonic evolution of the Himalayan orogen as constrained by along-strike variation of structural geometry, exhumation history, and foreland sedimentation. *Earth Sci Rev* 76:1–131.
26. Webb AAG, et al. (2011) Cenozoic tectonic history of the Himachal Himalaya (northwestern India) and its constraints on the formation mechanism of the Himalayan orogen. *Geosphere* 7:1013–1061.
27. Ali JR, Aitchison JC (2005) Greater India. *Earth Sci Rev* 72:169–188.
28. Aitchison J, Xia X, Baxter AT, Ali JR (2011) Detrital zircon U-Pb ages along the Yarlung-Tsangpo suture zone, Tibet: Implications for oblique convergence and collision between India and Asia. *Gondwana Res* 20:691–709.
29. Dupont-Nivet G, Lippert P, van Hinsbergen DJJ, Meijers MJM, Kapp P (2010) Paleolatitude and age of the Indo-Asia collision: Paleomagnetic constraints. *Geophys J Int* 182:1189–1198.
30. Patzelt A, Li H, Wang J, Appel E (1996) Palaeomagnetism of Cretaceous to Tertiary sediments from southern Tibet: Evidence for the extent of the northern margin of India prior to the collision with Eurasia. *Tectonophysics* 259:259–284.
31. Yi Z, Huang B, Chen J, Chen L, Wang H (2011) Paleomagnetism of early Paleogene marine sediments in southern Tibet, China: Implications to onset of the India–Asia collision and size of Greater India. *Earth Planet Sci Lett* 309:153–165.
32. Hu X, et al. (2010) Provenance of Lower Cretaceous Wölong volcaniclastics in the Tibetan Tethyan Himalaya: Implications for the final breakup of Eastern Gondwana. *Sediment Geol* 223:193–205.
33. Jadoul F, Berra F, Garzanti E (1998) The Tethys Himalayan passive margin from Late Triassic to Early Cretaceous (South Tibet). *J Asian Earth Sci* 16:173–194.
34. Torsvik TH, Müller RD, Van der Voo R, Steinberger B, Gaina C (2008) Global plate motion frames: Toward a unified model. *Rev Geophys* 46:RG3004.
35. Stampfli GM, Hochard C (2009) Plate tectonics of the Alpine realm. *Ancient Orogens and Modern Analogues*, eds JB Murphy, JD Keppie, and AJ Hynes (Geological Society, London), Special Publication, Vol 327, pp 89–111.
36. Capitanio FA, Morra G, Goes S, Weinberg RF, Moresi L (2010) India–Asia convergence driven by the subduction of the Greater Indian continent. *Nat Geosci* 3:136–139.
37. Clift P, Vannucchi P (2004) Controls on tectonic accretion versus erosion in subduction zones: Implications for the origin and recycling of the continental crust. *Rev Geophys* 42:RG2001.
38. van der Voo R, Spakman W, Bijwaard H (1999) Tethyan slabs under India. *Earth Planet Sci Lett* 171:7–20.
39. Replumaz A, Negredo AM, Villasenor A, Guillot S (2010) Indian continental subduction and slab break-off during Tertiary collision. *Terra Nova* 22:290–296.
40. Hafkenscheid E, Wortel MJR, Spakman W (2006) Subduction history of the Tethyan region derived from seismic tomography and tectonic reconstructions. *J Geophys Res* 111:B08401.
41. Zhao J, et al. (2010) The boundary between the Indian and Asian tectonic plates below Tibet. *Proc Natl Acad Sci USA* 107:11229–11233.
42. van der Meer DG, Spakman W, van Hinsbergen DJJ, Amaru ML, Torsvik TH (2010) Toward absolute plate motions constrained by lower mantle slab remnants. *Nat Geosci* 3:36–40.
43. Caddick MJ, et al. (2007) Burial and exhumation history of a Lesser Himalayan schist: Recording the formation of an inverted metamorphic sequence in NW India. *Earth Planet Sci Lett* 264:375–390.
44. Imayama T, et al. (2012) Two-stage partial melting and contrasting cooling history within the Higher Himalayan Crystalline Sequence in the far-eastern Nepal Himalaya. *Lithos* 134–135:1–22.
45. Wang C, et al. (2008) Constraints on the early uplift history of the Tibetan Plateau. *Proc Natl Acad Sci USA* 105:4987–4992.
46. Molnar P, Lyon-Caen H (1988) Some simple physical aspects of the support, structure, and evolution of mountain belts. *Spec Pap Geol Soc Am* 218:179–207.
47. Sobel ER, Chen J, Heermance RV (2006) Late Oligocene-Early Miocene initiation of shortening in the Southwestern Chinese Tian Shan: Implications for Neogene shortening rate variations. *Earth Planet Sci Lett* 247:70–81.
48. Lease RO, et al. (2011) Middle Miocene reorganization of deformation along the northeastern Tibetan Plateau. *Geology* 39:359–362.
49. Johnson MRW (2002) Shortening budgets and the role of continental subduction during the India–Asia collision. *Earth Sci Rev* 59:101–123.
50. Clift PD, et al. (2008) Correlation of Himalayan exhumation rates and Asian monsoon intensity. *Nat Geosci* 1:875–880.
51. Yin A, et al. (2010) Geologic correlation of the Himalayan orogen and Indian craton: Part 2. Structural geology, geochronology, and tectonic evolution of the Eastern Himalaya. *Geol Soc Am Bull* 122:360–395.
52. Gradstein FM, et al. (1994) A Mesozoic time scale. *J Geophys Res* 99:24051–24074.
53. Cande SC, Kent DV (1995) Revised calibration of the geomagnetic polarity timescale for the Late Cretaceaous and Cenozoic. *J Geophys Res* 100:6093–6095.
54. O'Neill C, Muller D, Steinberger B (2005) On the uncertainties in hot spot reconstructions and the significance of moving hot spot reference frames. *Geochem Geophys Geosyst* 6:Q04003.
55. Amaru ML (2007) Global travel time tomography with 3-D reference models. PhD thesis *Geol Ultraiectina*, 274 (Utrecht Univ, Utrecht, The Netherlands).

# Supporting Information

## van Hinsbergen et al. 10.1073/pnas.1117262109

### SI Text

**Paleomagnetic Constraints on the Age of the India–Asia Collision and Size of Greater India.** The relative positions of continents that are directly connected by ocean basins are determined by plate circuits based on marine magnetic anomalies and fracture zones (1). The paleolatitude of a continent is paleomagnetically determined from global synthetic apparent polar wander paths (APWPs), which are obtained by rotating all available high-quality paleomagnetic poles using Euler poles from the plate circuit to a chosen reference location (2, 3). This paper uses the most recent global synthetic APWP of Torsvik et al. (3), which covers the last 320 Ma. The global synthetic APWP (3) did not include the minor changes in the Indo-Atlantic plate circuit of van Hinsbergen et al. (4) used in our plate reconstruction. These changes, however, do not significantly influence the analyses below. From 320 to 440 Ma, the analysis below uses the APWPs for Gondwana and Laurasia of Torsvik and van der Voo (5), and before 440 Ma, uses the Gondwana poles from Torsvik et al. (6). These APWPs are determined for individual continents based on paleomagnetic poles of that continent alone.

The global synthetic APWPs do not include poles from continental blocks that are not bounded (or not anymore) by oceans, but are now instead separated by deformed belts, such as the northern edge of Greater India (i.e., the Himalaya) and the southern edge of Greater Asia (i.e., the Tibetan orogen). These blocks are frequently internally deformed by shortening and may have experienced regional and local vertical axis rotations during tectonism. Although paleomagnetic data from these deformed blocks cannot be used in APWP compilations, the inclination component can be used to calculate the paleolatitude of these blocks through time for comparison with plates in the plate circuit.

We assess the relative paleolatitude of the Indian and Siberian cratons that bound the India–Asia collision zone by using the APWPs described above to calculate the predicted paleolatitude of a reference location presently located on the Indus–Yarlung Suture Zone (IYSZ) for each continent (29°N, 88°E) (Table S1). We test the accuracy of these APWP predictions with paleolatitudes for the reference location calculated from robust lava-based paleomagnetic poles from cratonic India. We then add paleomagnetic information from rocks directly bordering the IYSZ, that is, paleomagnetic poles determined from lavas and sediments from the Lhasa and Qiangtang blocks and the Tibetan Himalaya. The selection of poles from the Lhasa and Qiangtang blocks, the Tibetan Himalaya, and cratonic India are described below, with sampling localities shown in Fig. S1.

**Paleomagnetic Data Procedures.** A robust paleomagnetic pole is calculated from primary, well-determined, independent readings of the geomagnetic field over a time period that is long enough to average the effect of paleosecular variation of the geomagnetic field, but short enough so as to not integrate appreciable plate motion. It is generally assumed that continuous sections of sedimentary rocks average secular variation, such that a stratigraphic series of site mean directions, or a magnetostratigraphic column, will provide a good characterization of the magnetic field. This assumption is only valid, however, if the preserved magnetic directions (*i*) are primary and (*ii*) have not been biased by sedimentary inclination shallowing caused by particle settling and compaction (7, 8). When magnetic directions are collected at the site level (in contrast to a continuous stratigraphic succession in magnetostratigraphic studies), site mean directions must be of comparable reliability before they can be transformed to virtual geomagnetic poles (VGPs) to calculate the average paleomagnetic pole at a study location. In the compilations below, we apply the following filtering criteria to site mean directions determined from sedimentary rocks, by excluding sites that (*i*) are not used by the original authors, if reason for exclusion is provided; (*ii*) contain directions of mixed polarity [i.e., a single sample of the geomagnetic field (site mean direction) should be short enough to exclude a reversal event]; (*iii* ) are characterized by fewer than five samples; (*iv*) have $\alpha_{95}$ values (the radius of the 95% confidence interval on the mean direction) greater than 20°; (*v*) or deviate more than 45° from the locality mean direction.

Paleomagnetic results from lavas must be treated differently than results from sediments, because the processes and timescales by and over which magnetic directions are recorded are principally different. Several independent readings of the geomagnetic field are required to accurately characterize its time-averaged behavior, which is fundamental to determining a robust paleomagnetic pole. Cooling of a single, thin (1–3 m) lava unit will record a geologically instantaneous measurement of the geomagnetic field. Furthermore, subsequent lavas can extrude within a short time period (years), such that several stratigraphically successive lavas often record the same magnetic field direction, meaning that each lava unit may not provide an independent reading of the geomagnetic field. Hence, paleomagnetic data from volcanic units must first be filtered so that all site mean directions are of comparably high quality, and then, if the sampling strategy permits, stratigraphically successive site mean directions that are statistically indistinguishable should be combined into direction groups. In the compilations below, we apply the following filtering criteria to site mean directions determined from lavas by excluding sites that (*i*) are not used by the original authors, if reason for exclusion is provided; (*ii*) contain directions of mixed polarity; (*iii*) are characterized by fewer than five samples; (*iv*) have k values (Fisher's precision parameter, ref. 9) less than 50; (*v*) or deviate more than 45° from the mean site mean direction.

This filtering procedure is commonly used by the geomagnetic field community (10, 11). The assignment of direction groups follows from the original authors of each of the studies described below, and in general follows the procedures described by Dupont-Nivet et al. (12) and Lippert et al. (13).

Paleomagnetic studies of the present and ancient magnetic field indicate that VGPs fit a Fisherian distribution better than the parent directions (11, 14). Therefore, we transform site mean and direction group directions into VGPs and calculate the Fisher mean VGP for each sampling locality. We evaluate the averaging of secular variation of a mean lava-based VGP by comparing the calculated dispersion (S) of VGPs to the dispersion observed in ancient lavas that yield good estimates of a geocentric axial dipole field when averaged (11, 14), and to the dispersion determined from paleosecular variation models (15). If the dispersion of the VGPs is consistent with dispersion observed in young lava successions, then we conclude that the sample set represents and has averaged secular variation.

We calculate the expected inclination and its uncertainty at the reference location on the IYSZ (29°N, 88°E), as well as the expected paleolatitude and corresponding uncertainty of the reference locality from each tilt-corrected locality paleomagnetic pole following Butler (16). Paleomagnetic poles, predicted inclinations, and paleolatitudes are listed in Table S1. All age assignments follow the original authors unless otherwise noted and are

keyed to the same timescales as used in the global synthetic APWP (3), that is, Gradstein et al. (17) and Cande and Kent (18), unless the section is dated using radiometric techniques.

**Paleomagnetic Poles Used in This Study.** ***Paleomagnetic poles from cratonic India.*** Two robust paleomagnetic poles from the Rajmahal ($118 \pm 1$ Ma) and Deccan ($65 \pm 1$ Ma) Traps on cratonic India are recalculated based on the most recent paleomagnetic data. These poles are used to test the accuracy of the global synthetic APWP (3) for predicting Indian paleolatitudes.

***The Deccan Traps.*** The end-Cretaceous Deccan Traps in western India have been the focus of many paleomagnetic (see reviews by Vandamme et al., ref. 19, and Chenet et al. ref. 20) and geochronologic (see reviews by Hofmann et al., ref. 21, and Chenet et al., ref. 22) studies. High-precision $^{40}Ar/^{39}Ar$ geochronology consistently yield eruption ages of $65 \pm 1$ Ma for the Deccan Traps, indicating that the >3-km thick unit erupted rapidly, but still spans several Ma. Paleomagnetic data from the Deccan Traps (19, 20, 23) (Tables S2–S4) should therefore sample sufficient time to accurately characterize secular variation of the geomagnetic field but not so much time that the rapid northward motion of India is of concern.

For the exceptionally large and high-quality dataset of Chenet et al. (20), we recalculated the single eruptive event directions assigned by the original authors by (*i*) selecting only site mean directions that met our quality criteria (Table S2), then (*ii*) recalculating direction group directions as assigned by the original authors using these filtered data (Table S3), and (*iii*) finally by recalculating the single eruptive events as assigned by the original authors in pole space. These new single eruptive event directions, as well as site mean directions from Vandamme et al. (19, 23) (Table S4) that met our quality criteria, are shown in Table S5. Paleomagnetic directions from these latter two studies have not been binned into direction groups due to lack of detailed stratigraphic information and may contain duplicate spot readings of the geomagnetic field. The 65 VGPs resulting from the site mean directions that pass our data quality filter provide a paleomagnetic pole for the Deccan Traps located at 37.1°N, 285.3°E ($A_{95} = 3.3°$, $K = 29.7$, $S = 14.9°$). Although the position of this paleomagnetic pole is not statistically different from previous Deccan poles (19, 20), the VGP scatter is more consistent with secular variation studies of young lavas at the same latitude (11).

The $65 \pm 1$ Ma paleolatitude of the reference location on the IYSZ calculated from this pole is $-21.9 \pm 3.3$ °N, in contrast to the more northerly $-15.1 \pm 2.4$ °N latitude calculated from the coeval Indian APWP pole. We prefer to use the Deccan pole as the cratonic Indian reference pole over the coeval Indian APWP pole because it is based on direct measurements of well-dated lava units on the Indian craton and is one of the most robust paleomagnetic poles in the geologic record. The Deccan pole therefore overcomes potential uncertainties in the global synthetic APWP caused by (*i*) small errors in the relative plate motions between continents; (*ii*) the inclusion of paleomagnetic poles in the compilation with unrecognized errors, for instance due to sedimentary inclination shallowing biases or insufficient averaging of secular variation in volcanic-based datasets; and (*iii*) the relatively low number of individual poles used in each averaging window. Further discussion on uncertainties in synthetic APWPs can be found elsewhere (3, 12, 13, 24, 25).

***The Rajmahal Traps.*** The Aptian Rajmahal Traps of eastern India have been accurately dated to $118 \pm 1$ Ma using single-crystal argon geochronology (26). Paleomagnetic results from the Rajmahal Traps are published by Klootwijk (27) and Sherwood and Malik (28) and are presented in Table S6. Thirty-three of the 48 site mean directions met our quality criteria, resulting in a paleomagnetic pole located at 8.1°N, 297.9°E ($A_{95} = 4.1°$, $K = 37.4$, $S = 13.3°$). The calculated dispersion of the VGPs can be straightforwardly explained by secular variation typical for the Cretaceous Superchron (14). The $118 \pm 1$ Ma paleolatitude of the reference location on the IYSZ calculated from this pole for cratonic India is $-43.0 \pm 4.1$ °N. This paleolatitude is statistically indistinguishable from the $-43.4 \pm 2.6$ °N latitude predicted by the global synthetic APWP (3).

**Paleomagnetic Poles from Southern Tibet (Greater Asia).** ***Eocene-Oligocene lavas.*** Paleomagnetic data from well-dated upper Eocene-lower Oligocene ($35 \pm 3$ Ma) basaltic lavas from the Qiangtang block are described by Lippert et al. (13). Thirty-three site mean directions from three sampling localities have been filtered and binned into 20 independent direction groups with a dispersion that is consistent with modern secular variation studies. These lavas yield a maximum likelihood estimate of paleolatitude of $28.7 \pm 3.7$ °N at a present reference site at 33°N, 88°E on the Lhasa-Qiangtang suture. Because there has been negligible north-south-directed upper crustal shortening or rotation within the Lhasa block throughout the Neogene (29–31), we can transfer this paleolatitude directly to our reference position on the IYSZ, 4° of latitude to the south, resulting in a paleolatitude estimate for the reference location of $24.7 \pm 3.8$ °N at approximately $35 \pm 3$ Ma.

***Paleogene lavas.*** Basaltic to andesitic lavas, tuffs, and volcanoclastic units of the upper Paleocene to lower Eocene (56–47 Ma) Linzizong formation (LZF) blanket a large area of the southern Lhasa block (32, 33). These volcanic units have been the focus of several paleomagnetic studies because of their potential to reveal the paleolatitude of the southern margin of Asia at approximately 56–47 Ma (Fig. S1) (34–39). Paleolatitude estimates for the reference location on the IYSZ from these individual studies range from approximately 12°N to as high as approximately 32°N, mainly as a result of the low number of independent site mean directions in each study.

We compiled all reliable data from the six studies of the upper LZF (i.e., Pana and upper Nianbo formations) listed above. After applying the data quality filter described above, excluding 37 of 89 reported lava site mean directions, the mean paleomagnetic pole in tilt-corrected coordinates is located at 80.1°N, 248.6°E ($K = 26.8$, $A_{95} = 3.9°$, $S = 15.7°$, $n = 52$). The 52 site mean directions used to calculate this filtered paleomagnetic pole include data from each of the six independent studies, pass a reversal test at 95% confidence (class C: $Y_{\text{calculated}} = 7.6°$, $Y_{\text{critical}} = 10.9°$; ref. 40), and pass a regional fold test at 95% and 99% confidence ($X_2$ test of McFadden, ref. 41) (Table S7). Importantly, the calculated dispersion of this filtered VGP is consistent with known dispersion caused by paleosecular variation (11). We conclude that this paleopole more accurately characterizes the time-averaged behavior of the geomagnetic field than any previous individual study of the LZF. The 56–47 Ma paleolatitude of the reference site on the IYSZ predicted from this pole is $19.6 \pm 3.9$ °N.

Some recent studies (36) have reported reconnaissance paleomagnetic data from the lower LZF (approximately 64–60 Ma), suggesting paleolatitudes as low as $6.6\,°N \pm 8.5\,°N$ (reference locality 30.0°N, 91.2°E). These anomalously low latitudes would imply unlikely large and fast northward motion (>1,500 km) of southern Tibet from 60 to 50 Ma, the evidence for which is either lacking or remains unrecognized. These results are based on a limited number of sites from which our data quality filter removes too many site mean directions to provide a statistically robust paleomagnetic pole. We therefore choose to not incorporate these data into our compilation.

***Upper Cretaceous redbeds, Maxiang.*** Sun et al. (42) report paleomagnetic data from the 100–72 Ma Shexing formation of redbeds that outcrop along the Lhasa-Golmud highway near Maxiang.

Site mean directions calculated from the high-temperature characteristic remanent magnetization (ChRM) component pass a fold test at high confidence. We evaluated the distribution of high-temperature specimen directions for inclination shallowing following the elongation/inclination (E/I) method of Tauxe and Kent (15). Samples with mean angular deviations of ChRM directions >15° and with reversed polarity ChRM directions were removed from the population to exclude poorly resolved or transitional directions. The Vandamme cutoff procedure for identifying outliers in the direction population (43) removed another seven samples, resulting in a mean direction of the Shexing formation with declination = 343.4°, inclination = 31.2° ($\alpha_{95}$ = 2.8°, $k$ = 26.7, $n$ = 100) (Fig. S3*A*). We calculated a flattening factor of 0.66 (0.53 and 0.91 95% confidence interval), resulting in an E/I corrected inclination of 40.5° (33.3–47.7° 95% confidence interval) (Fig. S3 *C* and *D*). These results indicate approximately 9° of inclination shallowing in the fluvial-lacustrine redbeds of the Shexing formation, which is typical of these facies in Asia (12, 13). The formation mean direction calculated from the E/I-corrected directions is declination = 343.4°, inclination = 41.6°, $\alpha_{95}$ = 2.8°, $k$ = 26.0, $n$ = 100 (Fig. S3*B*), with a corresponding pole at 74.1°N, 342.7°E ($A_{95}$ = 2.3). The calculated paleolatitude for the reference location on the IYSZ is 23.8 ± 2.3 °N at 100–72 Ma, which is consistent with E/I-corrected data from upper Cretaceous redbeds from the Penbo regions of the Lhasa terrane (see below).

***Upper Cretaceous redbeds, Penbo.*** We use paleomagnetic data from the nonmarine Takena formation and calculations of a late Cretaceous (105–90 Ma, ref. 44) paleolatitude for the Lhasa Block of Tan et al. (34). The distribution of the sample directions from this dataset are consistent with inclination shallowing that is readily attributed to sedimentary depositional processes. These directions have been corrected by Tan et al. (34) using the E/I method (15). The paleomagnetic pole calculated from these tilt and inclination shallowing corrected sediments is located at 79.6°N, 329.9°E ($A_{95}$ = 2.2). The paleolatitude of the reference location on the IYSZ in Lhasa-terrane coordinates calculated from this pole is 23.7 ± 2.2 °N at approximately 105–90 Ma.

***Lower Cretaceous Lavas.*** Paleomagnetic results from volcanic rocks of Cretaceous age have been reported in two recent studies. Sun et al. (45) describe 15 site mean directions from the 114.2 ± 1.1 Ma Woronggou formation rhyolites near Deqing, on the west shore of Nam Co (Table S8). Ten site mean directions have either too few samples defining the site mean direction or precision parameters <50, leaving only five directions for further analysis. Chen et al. (46) describe 19 site mean directions from 130–110 Ma tuffs and lavas of the Zenong Group near the town of Cuoqin in the central Lhasa terrane (Table S8). Nine of these site mean directions have precision parameters <50°, and another direction is considered an outlier by the original authors, leaving only nine site mean directions to describe the geomagnetic field at this locality. We combine the filtered results of Sun et al. (45) and Chen et al. (46) to calculate a lava-based paleomagnetic pole for the Lower Cretaceous of the Lhasa terrane. Although both localities show similar inclinations, the declinations vary by approximately 30–40°, indicating significant rotations between the localities (Fig. S4). We follow Doubrovine and Tarduno (24) and Lippert et al. (13), and calculate a maximum likelihood virtual geomagnetic latitude (VGL) using the Arason and Levi method (47). First, we calculate the VGPs for the filtered site mean directions and then calculate the VGL of the reference site on the IYSZ. These VGLs are then used as input to calculate the maximum likelihood latitude for the reference site from these data: 16.2 ± 3.6 °N at approximately 130–110 Ma. We note, however, that the dispersion of these VGLs is only 7.0°, indicating that paleosecular variation has been undersampled by these igneous units, and that this paleolatitude estimate may not be robust. Additional paleomagnetic studies focusing on Cretaceous volcanic rocks from the Lhasa terrane are clearly warranted.

***General comment on paleomagnetism of Cretaceous rocks of the Lhasa terrane.*** We note that many historical paleomagnetic studies of Cretaceous rocks of the Lhasa terrane have been excluded from our compilation; for example, Achache et al. (35), Pozzi et al. (48), Westphal and Pozzi (49), Lin and Watts (50), and Chen et al. (51). The reasons for these exclusions are because (*i*) most of these studies produced very small sample sets with few site mean directions such that paleosecular variation and inclination shallowing could not be evaluated; and (*ii*) the more recent studies that we summarize above supersede all of these previous studies in terms of paleomagnetic field tests, rock magnetic tests, and overall data quality.

**Paleomagnetic Poles from the Tibetan Himalaya (Greater India).** Below, we summarize all available paleomagnetic poles for the Tibetan Himalaya (Fig. S1). Inclination shallowing corrections are only available for the late Cretaceous to Paleocene poles. Poles of early Cretaceous and older age have not been corrected for inclination shallowing, and the effects of sedimentary inclination shallowing on the paleolatitude estimations require future work. We note, however, that the effect of possible inclination shallowing can only decrease the paleomagnetically estimated size of Greater India, as its Paleozoic to Cretaceous position was exclusively on the southern hemisphere. Moreover, the majority of paleomagnetic data from the Triassic Tibetan Himalaya are from marine limestones, which typically show only small (<5°) amounts of inclination shallowing (12, 52).

Several coeval Tibetan Himalaya poles plot east or west of the Indian APWP. This relationship indicates significant, locality-specific vertical axis rotation of Tibetan Himalayan rocks with respect to the Indian craton. These tectonic rotations must postdate the age of the rocks in which they are found and probably accrued during the intense deformation of the Tibetan Himalaya that began with the obduction of ophiolites during the latest Cretaceous to early Paleogene (53, 54) and continued during the collision of the Tibetan Himalaya with the Lhasa block (12, 55–58). We are primarily interested in the latitudinal separation between the Tibetan Himalaya and cratonic India, so here we correct for these vertical axis rotations by moving the Tibetan Himalayan pole by an angular distance equal to the rotation of the Tibetan Himalayan pole with respect to the coeval pole from cratonic India (e.g., Indian APWP or Deccan or Rajmahal poles) about a small circle that is centered on the sampling site for the Tibetan Himalayan pole. The rotation-corrected Tibetan Himalayan poles are used to calculate the paleolatitudes shown in Fig. 2 of the main paper, Fig. S2, and Table S1, and are shown in Fig. S5; the inclination and paleolatitude estimates from the uncorrected poles are shown for comparison in Table S1. We note that accounting for these vertical axis rotations typically changes the paleolatitude estimates by less than one degree.

***Upper Cretaceous–upper Paleocene marine sediments.*** Paleomagnetic data from the Maastrichtian to Paleocene Zongshan and Selandian-Thanetian Zongpu formations near Gamba and Duela in Southern Tibet are described by Patzelt et al. (59) and Yi et al. (52). Both datasets pass paleomagnetic fold tests and reversal tests at high confidence as described in the original studies, consistent with a primary magnetization. Dupont-Nivet et al. (12) tested the sediment-based data of Patzelt et al. (59) using the E/I procedure and found only minor (<5°) amounts of inclination shallowing, as common for marine limestones. Yi et al. (52) also evaluated their data using the E/I procedure and also found minor (4.4°) inclination shallowing. Here we combine the ChRM specimen directions of Patzelt et al. (59) and Yi et al. (52) from

the Zongpu formation to recalculate the magnitude of inclination shallowing. Tilt-corrected outlier directions in this combined dataset were removed using the Vandamme cutoff criteria (43), resulting in 245 individual directions that define a slightly elongated distribution (Fig. S6*A*). This filtered dataset passes a reversals test at high confidence ($Y = 2.4°$, $Y_c = 12.0°$, class C) (40). We calculated a flattening factor of 0.69 (0.61% and 0.80 95% confidence interval), resulting in an E/I-corrected inclination of 15.6° (12.6–18.5° 95% confidence interval) (Fig. S6 *C* and *D*). These results indicate approximately 4° of inclination shallowing in the marine limestones of the Zongpu formation. Two outlier directions were removed from the population of E/I-corrected directions, resulting in a formation mean direction of declination = 358.6°, inclination = 15.5°, $a_{95} = 2.3°$, $k = 16.6$, $n = 243$ (Fig. S6*B*). The corresponding poles for the Zongpu formation calculated from this direction, as well as the for the Zongshan formation previously calculated by Dupont-Nivet et al. (12) are shown in Table S1. We calculate a paleolatitude for the reference location on the IYSZ of 8.7 ± 1.7 °N with an age range of 62–56 Ma, and −5.0 ± 2.8 °N for 71–65 Ma (12). The age of the Zongpu formation latitude is constrained by recent magnetostratigraphy (52). The upper Cretaceous pole is rotated east of the Indian APWP, however, and the rotation-corrected paleolatitude at 71–65 Ma is −4.9 ± 2.8 °N. Compared to the Indian APWP, the Zongpu pole (59 ± 3 Ma) shows 16.6 ± 2.9° of latitudinal distance between India and the Tibetan Himalaya, whereas the Zongshan pole (68 ± 3 Ma) indicates 13.6 ± 4.4° of latitudinal separation. (Fig. 2 and Figs. S2 and S5) (12).

***Cretaceous volcanoclastic sediments.*** Klootwijk and Bingham (58) sampled the Barremian to late Albian (127–112 Ma) Dzong formation in the Thakkhola graben. Ninety-five paleomagnetic samples from the lower glauconitic sandstone part of the formation, which has been assigned an Aptian age (121–112 Ma) (60), pass a paleomagnetic fold test at high confidence (58). These data were used to calculate a paleomagnetic pole located at −12.0 °N, 108.6°E ($A_{95} = 3.7°$). This pole is located east of the coeval Indian APWP pole, indicating significant rotation of the Tibetan Himalaya with respect to cratonic India sometime after the deposition of the Dzong formation. The rotation-corrected paleolatitude is −45.1 ± 3.7 °N; for comparison, the uncorrected paleolatitude is −44.4 ± 3.7 °N. Both of these estimates overlap within error with the coeval Indian APWP pole and the cratonic India pole from the Rajmahal Traps. Notably, the paleolatitude difference between rotation-corrected Dzong pole calculation and the Rajmahal pole prediction is −2.1 ± 5.5° of latitude.

***Triassic marine sediments.*** Paleomagnetic data from Triassic strata throughout the Tibetan Himalaya were collected from several published sources (Fig. S1 and Table S9). Stratigraphic nomenclature follows the original authors, whereas stage assignments follow Garzanti (60), and stage ages follow Gradstein et al. (17).

Klootwijk et al. (61) describe paleomagnetic results from six sampling localities from Kashmir in the western Tibetan Himalaya. Sampled lithologies include marine limestone, shales, and sandstones of lowest Induan to Norian age (i.e., 248.2–209.6 Ma). Most samples revealed high-temperature ChRM interpreted as primary in tilt-corrected coordinates. The mean VGP calculated from these six localities gives a paleolatitude of −55.2 ± 8.7 °N for the reference location on the IYSZ. The Kashmir pole shows a large rotation from the Indian APWP. The rotation-corrected paleolatitude for the reference location is −49.6 ± 8.7 °N.

Induan to early Norian (248.2–215 Ma) greenschist-facies meta-shales and limestones of the Tamba and Mukut formations from the western Dolpo region of the Tibetan Himalaya record a high-temperature magnetization carried by magnetite and interpreted to be prefolding in age (62). Ten of the 26 site mean directions meet our quality criteria. A new paleomagnetic pole calculated from the 10 corresponding VGPs is located at −2.9 °N, 281.4°E ($A_{95} = 18.5°$, $K = 7.8$), but is located east of the Indian APWP. The rotation-corrected paleolatitude for the reference location is −55.9 ± 18.5 °N. This paleolatitude is the most southerly in this compilation, lying more than 25° of latitude south of the APWP prediction. According to this pole, the Tibetan Himalaya (TH) was derived from the center of the Indian craton; this is geologically implausible. We choose to exclude these Dolpo results from our compilation given the large number of sites rejected, the low number of samples, the greenschist-facies metamorphism of the limestones, and the weak fold test used to suggest a primary magnetization. Future paleomagnetic sampling of Triassic and younger rocks in the Dolpo region are needed to verify these results.

Paleomagnetic results from two sampling localities in the Ladinian to Norian (234.3–209.6 Ma) Thinigaon Limestone of the Thakkhola region are described by Klootwijk and Bingham (58). A high-temperature ChRM is resolved in most samples and is interpreted to be primary in tilt-corrected coordinates. The mean VGPs calculated from these two localities show only small rotation with respect to India. The rotation-corrected paleolatitude estimates for the reference location are −30.1 ± 5.7 °N and −26.9 ± 10.0 °N.

Lower Anisian to lower Norian (241.7–215 Ma) carbonates from a single sampling locality near the Manang area of the Tibetan Himalaya record a ChRM carried by magnetite (63). A positive fold test of the ChRMs suggests that these directions are primary and suitable for calculating a paleomagnetic pole. This pole shows only minor rotation of the Manang region with respect to cratonic India since the Triassic. The rotation-corrected paleolatitude of the reference location is −36.2 ± 4.2 °N.

Thirty-four paleomagnetic sampling sites collected from the lowest Induan to Norian (248.2–209.6 Ma) limestones of the Tomba Kurkur and Mukut formations of Central Nepal are described by Schill et al. (64). A high-temperature component carried by magnetite was interpreted as primary by these authors. Thirteen of these site mean directions meet our quality criteria, resulting in a mean VGP located at 14.1°N, 256.3°E ($A_{95} = 10.8°$, $K = 15.7$). This pole is rotated east of the coeval Indian APWP. The rotation-corrected paleolatitude of the reference location is −47.5 ± 10.8 °N.

In summary, paleomagnetic data from several different packages of Triassic rocks distributed throughout the Tibetan Himalaya record stable, primary remanences. The paleomagnetic poles from each of the sampling locations indicate differential amounts of vertical axis rotation with respect to cratonic India. We use the rotation-corrected paleolatitudes from each of the studies (excluding the results from Dolpo) described above to calculate the maximum likelihood paleolatitude (47) of the reference site in a Tibetan Himalaya reference frame of −38.6 ± 9.9 °N. In contrast, the maximum likelihood estimate of the reference location calculated from the 250–200 Ma Indian APWP poles is −30.1 ± 6.9 °N (the paleolatitude calculated from the Fisher mean of the 250–200 Ma Indian APWP poles is −29.9 ± 7.3 °N). Thus, we find that the mean latitudinal separation between the reference location in a Tibetan Himalaya and cratonic India reference frame during the Triassic is −9.0 ± 10.6° (Fig. S5). We note that several individual poles of high quality lie closer to the Triassic APWP poles than indicated by this comparison of the maximum likelihood estimates.

***Ordovician redbeds.*** Paleomagnetic data from the Shian formation of the Tibetan Himalaya near Spiti, Northwest India are described by Torsvik et al. (6), who assigned an Ordovician (500–450 Ma) age to these rocks. High-temperature ChRM

directions carried by hematite pass a fold test at high confidence, and the six paleomagnetic sampling sites yield a mean VGP located at −20.4 °N, 210.0°E ($A_{95} = 13.4°$, $K = 26.0$) (Tables S1 and S10), which is rotated away from the coeval part of the Indian APWP. The paleolatitude of the reference location calculated from the rotation-corrected pole is −37.7 ± 13.4 °N.

**Implications of Paleomagnetic Data for the India–Asia Collision History.** ***Age of the Tibetan Himalaya–Lhasa collision.*** The paleolatitude separation between the late Cretaceous and Paleocene poles for the TH and the coeval Indian APWP poles is remarkably similar (23.6 ± 3.7° at 59 Ma; 20.4 ± 4.8° at 68 Ma, using the trend of the Indian APWP adjusted to the Deccan Traps paleopole), suggesting that over this time span, the Tibetan Himalaya drifted northward at a similar rate as cratonic India (Fig. 2 and Figs. S2 and S5). We use these paleolatitude separation values to calculate a mean latitudinal separation between the Tibetan Himalaya and cratonic India of 22.0 ± 3.0° from 65 to 59 Ma (Fig. S5). In other words, paleomagnetism shows that sometime after 59 Ma, 22.0 ± 3.0° of North–South (N-S) convergence occurred between the northernmost exposed tip of the Tibetan Himalaya, located at the modern suture zone, and continental India.

If we assume that there was no convergence accommodated within Greater India prior to collision with Eurasia, we can calculate a collision age by constructing a Tibetan Himalayan "APWP" (or better, paleolatitude curve, Fig. S2) that is parallel to the Indian APWP and is projected forward in time until it intersects with the Asian paleolatitude curve (specifically, the paleolatitude calculated from the Linzizong formation); the 95% uncertainty in latitude assigned to the Tibetan Himalayan APWP is ±3°. The latitude of the northern Tibetan Himalaya overlaps with the latitude of the southern margin of the Lhasa block at 48.6 ± 6.2 Ma at 19.6 ± 3.9 °N (95% confidence intervals, see Fig. 2 and Fig. S2).

***Paleolatitudinal drift of the Tibetan Himalaya relative to continental India.*** Paleolatitudes calculated from paleomagnetic data from Ordovician, Triassic, and lower Cretaceous sediments of the Tibetan Himalayan sequence all overlap within error with paleolatitudes predicted from coeval cratonic Indian reference poles (Figs. S2 and S5). This overlap means that the N-S area of 22.0 ± 3.0° that disappeared due to convergence within Greater India sometime after 59 Ma (probably after 48.6 ± 6.2 Ma, see above) must have been created by extension after approximately 120 Ma.

When making a direct comparison between the paleolatitude of the Rajmahal Traps (118 ± 1 Ma) and the Dzong formation of the Tibetan Himalaya (121–112 Ma) a statistically indistinguishable post-118 Ma net separation of −2.1 ± 5.5° of latitude (−233 ± 877 km N-S separation) is obtained. This value shows that the Greater India 118 Ma ago was not more than 644 km (i.e., 877–233 km) larger than today. Today's width of Greater India is equal to the width of the Himalaya—i.e., approximately 250 km. Hence, paleomagnetism constrains the maximum width (within 95% error bars) of Greater India 118 Ma ago at approximately 900 km. Using the 22.0 ± 3.0° of post-59 Ma convergence calculated above, the net increase in paleolatitudinal separation (i.e., the amount of N-S extension) between the Tibetan Himalaya and cratonic India implied by these direct comparisons is 24.0 ± 6.3° (2,675 ± 699 km N-S) between 118 and 68 Ma.

The estimated size of the Greater India Basin will be refined by future studies that provide robust paleomagnetic poles from Cretaceous rocks of the Tibetan Himalaya. Nevertheless, reviewing the current state-of-the-art of published, robust paleomagnetic data from India, the Tibetan Himalaya, and the Lhasa terrane indicate that the Tibetan Himalaya must have drifted away from cratonic India during the Cretaceous, leaving in its wake a basin or several basins that accommodated a cumulative N-S extension of 2,675 ± 699 km.


1. Cox A, Hart RB (1986) Plate tectonics: How it works (Blackwell Science, Oxford).
2. Besse J, Courtillot V (2002) Apparent and true polar wander and the geometry of the geomagnetic field over the last 200 Mya. *J Geophys Res* 107:2300.
3. Torsvik TH, Müller RD, Van der Voo R, Steinberger B, Gaina C (2008) Global plate motion frames: Toward a unified model. *Rev Geophys* 41:RG3004.
4. van Hinsbergen DJJ, Steinberger B, Doubrovine PV, Gassmöller R (2011) Acceleration and deceleration of India–Asia convergence since the Cretaceous: Roles of mantle plumes and continental collision. *J Geophys Res* 116:B06101.
5. Torsvik TH, van der Voo R (2002) Refining Gondwana and Pangea palaeogeography: Estimates of Phanerozoic non-dipole (octupole) fields *Geophys J Int* 151:771–794.
6. Torsvik TH, Paulsen TS, Hughes NC, Myrow PM, Ganerød M (2009) The Tethyan Himalaya: palaeogeographical and tectonic constraints from Ordovician palaeomagnetic data. *J Geol Soc* 166:679–687.
7. King RF (1955) The remanent magnetism of artificially deposited sediments. *Mon Not R Astron Soc* 7:115–134.
8. Tauxe L (2005) Inclination flattening and the geocentric axial dipole hypothesis. *Earth Planet Sci Lett* 233:247–261.
9. Fisher RA (1953) Dispersion on a sphere. *Proc R Soc London A* 217:295–305.
10. Deenen MHL, Langereis CG, van Hinsbergen DJJ, Biggin AJ (2011) Geomagnetic secular variation and the statistics of palaeomagnetic directions. *Geophys J Int* 186:509–520.
11. Johnson CL, et al. (2008) Recent investigations of the 0–5 Ma geomagnetic field recorded by lava flows. *Geochem Geophys Geosyst* 9:Q04032.
12. Dupont-Nivet G, van Hinsbergen DJJ, Torsvik TH (2010) Persistently shallow paleomagnetic inclinations in Asia: Tectonic implications for the Indo-Asia collision. *Tectonics* 29:TC5016.
13. Lippert PC, Zhao X, Coe RS, Lo C-H (2011) Palaeomagnetism and $^{40}Ar/^{39}Ar$ geochronology of upper Palaeogene volcanic rocks from Central Tibet: Implications for the Central Asia inclination anomaly, the palaeolatitude of Tibet and post-50 Ma shortening within Asia. *Geophys J Int* 184:131–161.
14. Biggin A, van Hinsbergen DJJ, Langereis CG, Straathof GB, Deenen MH (2008) Geomagnetic secular variation in the Cretaceous normal superchron and in the Jurassic. *Phys Earth Planet Int* 169:3–19.
15. Tauxe L, Kent DV (2004) A simplified statistical model for the geomagnetic field and the detection of shallow bias in paleomagnetic inclinations: Was the ancient magnetic field dipolar? *Timescales of the Paleomagnetic Field, Geophysical Monograph*, eds Channell JET, Kent DV, Lowrie W, Meert JG (American Geophysical Union, Washington, DC), Vol 145, pp 101–115.
16. Butler RF (1992) *Paleomagnetism: Magnetic Domains to Geologic Terranes* (Blackwell Scientific, Boston), pp 195.
17. Gradstein FM, et al. (1994) A Mesozoic time scale. *J Geophys Res* 99:24051–24074.
18. Cande SC, Kent DV (1995) Revised calibration of the geomagnetic polarity timescale for the Late Cretaceaous and Cenozoic. *J Geophys Res* 100:6093–6095.
19. Vandamme D, Courtillot V, Besse J, Montigny R (1991) Paleomagnetism and age determinations of the Deccan Traps (India): Results of a Nagpur-Bombay traverse and review of earlier work. *Rev Geophys* 29:159–190.
20. Chenet AL, et al. (2009) Determination of rapid Deccan eruptions across the Cretaceous-Tertiary boundary using paleomagnetic secular variation: 2. Constraints from analysis of eight new sections and synthesis for a 3500-m-thick composite section. *J Geophys Res* 114:B06103.
21. Hofmann C, Feraud G, Courtillot V (2000) $^{40}Ar/^{39}Ar$ dating of mineral separates and whole rocks from the Western Ghats lava pile: Further constraints on duration and age of the Deccan traps. *Earth Planet Sci Lett* 180:13–27.
22. Chenet AL, Quidelleur X, Fluteau F, Courtillot V, Bajpai S (2007) K-40-Ar-40 dating of the Main Deccan large igneous province: Further evidence of KTB age and short duration. *Earth Planet Sci Lett* 263:1–15.
23. Vandamme D, Courtillot V (1992) Paleomagnetic constraints on the structure of the Deccan traps. *Phys Earth Planetary Int* 74:241–261.
24. Doubrovine PV, Tarduno JA (2008) Linking the Late Cretaceous to Paleogene Pacific plate and the Atlantic bordering continents using plate circuits and paleomagnetic data. *J Geophys Res* 113:B07104.
25. Ganerød M, Smethurst MA, Rousse S, Torsvik TH, Prestvik T (2008) Reassembling the Paleogene-Eocene North Atlantic igneous province: New paleomagnetic constraints from the Isle of Mull, Scotland. *Earth Planet Sci Lett* 272:464–475.
26. Coffin MF, et al. (2002) Kerguelen hotspot magma output since 130 Ma. *J Petrol* 43:1121–1139.
27. Klootwijk CT (1971) Palaeomagnetism of upper Gondwana-Rajmahal Traps, Northeast India. *Tectonophysics* 12:449–461.
28. Sherwood GJ, Malik SB (1996) A palaeomagnetic and rock magnetic study of the northern Rajmahal volcanics, Bihar, India. *J Southeast Asian Earth Sci* 13:123–131.
29. Kapp P, Yin A, Harrison TM, Ding L (2005) Cretaceous-Tertiary shortening, basin development and volcanism in central Tibet. *Geol Soc Am Bull* 117:865–878.
30. Kapp P, et al. (2007) The Gangdese retroarc thrust belt revealed. *GSA Today* 17:4–9.
31. Kapp P, DeCelles PG, Gehrels GE, Heizler M, Ding L (2007) Geological records of the Cretaceous Lhasa-Qiangtang and Indo-Asian collisions in the Nima basin area, central Tibet. *Geol Soc Am Bull* 119:917–932.
32. He S, Kapp P, DeCelles PG, Gehrels GE, Heizler MT (2007) Cretaceous–Tertiary geology of the Gangdese Arc in the Linzhou area, southern Tibet. *Tectonophysics* 433:15–37.
33. Lee H-Y, et al. (2009) Eocene Neotethyan slab breakoff in southern Tibet inferred from the Linzizong volcanic record. *Tectonophysics* 477:20–35.

34. Tan X, et al. (2010) New paleomagnetic results from the Lhasa block: Revised estimation of latitudinal shortening across Tibet and implications for dating the India–Asia collision. *Earth Planet Sci Lett* 293:396–404.
35. Achache J, Courtillot V, Zhou YX (1984) Paleogeographic and tectonic evolution of southern Tibet since middle Cretaceous time: new paleomagnetic data and synthesis. *J Geophys Res* 89:10311–10339.
36. Chen J, Huang B, Sun L (2010) New constraints to the onset of the India–Asia collision: Paleomagnetic reconnaissance on the Linzizong Group in the Lhasa Block, China. *Tectonophysics* 489:189–209.
37. Sun Z, Jiang W, Li H, Pei JL, Zhu Z (2010) New paleomagnetic results of Paleocene volcanic rocks from the Lhasa block: Tectonic implications for the collision of India and Asia. *Tectonophysics* 490:257–266.
38. Dupont-Nivet G, Lippert P, van Hinsbergen DJJ, Meijers MJM, Kapp P (2010) Paleolatitude and age of the Indo-Asia collision: Paleomagnetic constraints. *Geophys J Int* 182:1189–1198.
39. Liebke U, et al. (2010) Position of the Lhasa terrane prior to India–Asia collision derived from palaeomagnetic inclinations of 53 Ma old dykes of the Linzhou Basin: Constraints on the age of collision and post-collisional shortening within the Tibetan Plateau. *Geophys J Int* 182:1199–1215.
40. McFadden PC, McElhinny MW (1990) Classification of the reversal test in palaeomagnetism. *Geophys J Int* 103:725–729.
41. McFadden PL (1990) A new fold-test for palaeomagnetic studies. *Geophys J Int* 103:163–169.
42. Sun Z, et al. (2012) Palaeomagnetism of late Cretaceous sediments from southern Tibet: Evidence for the consistent palaeolatitudes of the southern margin of Eurasia prior to the collision with India. *Gondwana Res* 21:53–63.
43. Vandamme D (1994) A new method to determine paleosecular variation. *Phys Earth Planet Int* 85:131–142.
44. Leier AL, DeCelles PG, Kapp P, Ding L (2007) The Takena formation of the Lhasa terrane, southern Tibet: The record of a Late Cretaceous retroarc foreland basin. *Geol Soc Am Bull* 119:31–48.
45. Sun Z, Jiang W, Pei JL, Li H (2008) New early Cretaceous paleomagnetic data from volcanic of the eastern Lhasa Block and its tectonic implications. *Acta Petrol Sin* 24:1621–1626.
46. Chen W, et al. (2012) Paleomagnetic results from the Early Cretaceous Zenong Group volcanic rocks, Cuoqin, Tibet, and their paleogeographic implications. *Gondwana Res* (in press).
47. Arason P, Levi S (2010) Maximum likelihood solution for inclination-only data in paleomagnetism. *Geophys J Int* 182:753–771.
48. Pozzi JP, Westphal M, Zhou YX, Xing SL, Chen XY (1982) Position of the Lhasa block, South Tibet, during the late Cretaceous. *Nature* 297:319–321.
49. Westphal M, Pozzi JP (1983) Paleomagnetic and plate tectonic constraints on the movement of Tibet. *Tectonophysics* 98:1–10.
50. Lin J, Watts DR (1988) Palaeomagnetic constraints on Himalayan-Tibetan tectonic evolution. *Philos Trans R Soc London* 326:177–188.
51. Chen Y, Cogné JP, Courtillot V, Tapponnier P, Zhu XY (1993) Cretaceous paleomagnetic results from western Tibet and tectonic implications. *J Geophys Res* 98:17981–17999.
52. Yi Z, Huang B, Chen J, Chen L, Wang H (2011) Paleomagnetism of early Paleogene marine sediments in southern Tibet, China: Implications to onset of the India–Asia collision and size of Greater India. *Earth Planet Sci Lett* 309:153–165.
53. Ding L, Kapp P, Wan X (2005) Paleocene-Eocene record of ophiolite obduction and initial India–Asia collision, south central Tibet. *Tectonics* 24:TC3001.
54. Searle MP, Treloar PJ (2010) Was Late Cretaceous—Palaeocene obduction of ophiolite complexes the primary cause of crustal thickening and regional metamorphism in the Pakistan Himalaya? *The Evolving Continents: Understanding Processes of Continental Growth*, eds Kusky TM, Zhai MG, Xiao W (Geological Society Special Publications, London), Vol 338, pp 345–359.
55. Murphy MA, Yin A (2003) Structural evolution and sequence of thrusting in the Tethyan fold-thrust belt and Indus-Yalu suture zone, southwest Tibet. *Geol Soc Am Bull* 115:21–34.
56. Ratschbacher L, Frisch W, Liu G, Chen CC (1994) Distributed deformation in southern and western Tibet during and after the India–Asia collision. *J Geophys Res* 99:19917–19945.
57. Schill E, Appel E, Zeh O, Singh VK, Gautam P (2001) Coupling of late-orogenic tectonics and secondary pyrrhotite remanences: towards a separation of different rotation processes and quantification of rotational underthrusting in the western Himalaya (northern India). *Tectonophysics* 337:1–21.
58. Klootwijk CT, Bingham DK (1980) The extent of greater India, III. Palaeomagnetic data from the Tibetan Sedimentary series, Thakkhola region, Nepal Himalaya. *Earth Planet Sci Lett* 51:381–405.
59. Patzelt A, Li H, Wang J, Appel E (1996) Palaeomagnetism of Cretaceous to Tertiary sediments from southern Tibet: Evidence for the extent of the northern margin of India prior to the collision with Eurasia. *Tectonophysics* 259:259–284.
60. Garzanti E (1999) Stratigraphy and sedimentary history of the Nepal Tethys Himalaya passive margin *J Asian Earth Sci* 17:805–827.
61. Klootwijk CT, et al. (1983) A palaeomagnetic reconnaissance of Kashmir, northwestern Himalaya, India. *Earth Planet Sci Lett* 63:305–324.
62. Crouzet C, Gautam P, Schill E, Appel E (2003) Multicomponent magnetization in western Dolpo (Tethyan Himalaya, Nepal): Tectonic implications. *Tectonophysics* 377:179–196.
63. Appel E, Müller R, Widder RW (1991) Palaeomagnetic results from the Tibetan sedimentary series of the Manang area (north central Nepal). Palaeomagnetic results from the Tibetan sedimentary series of the Manang area (north central Nepal). *Geophys J Int* 104:255–266.
64. Schill E, Appel E, Gautam P, Dietrich D (2002) Thermo-tectonic history of the Tethyan Himalayas deduced from the palaeomagnetic record of metacarbonates from Shiar Khola (Central Nepal). *J Asian Earth Sci* 20:203–210.

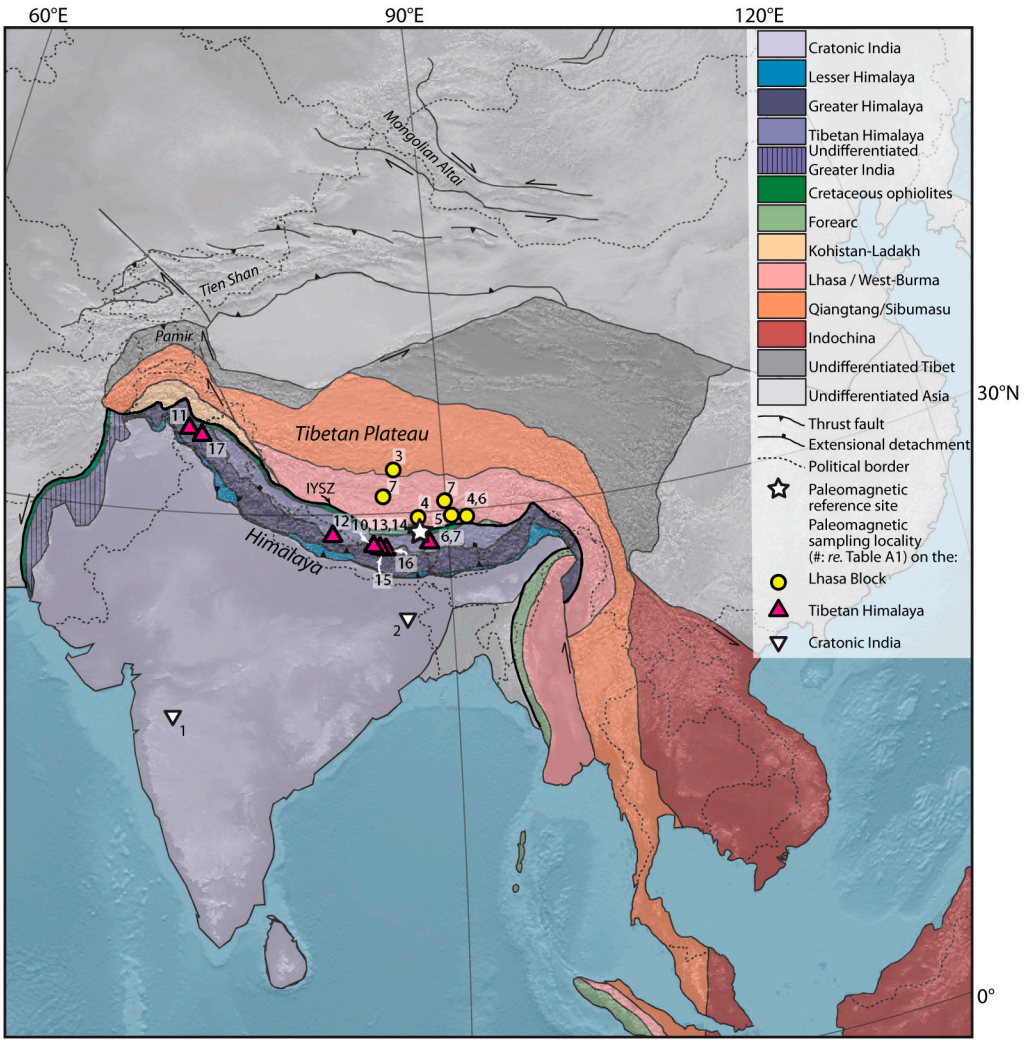


**Fig. S1.** Location map of paleomagnetic studies listed in Table S1.

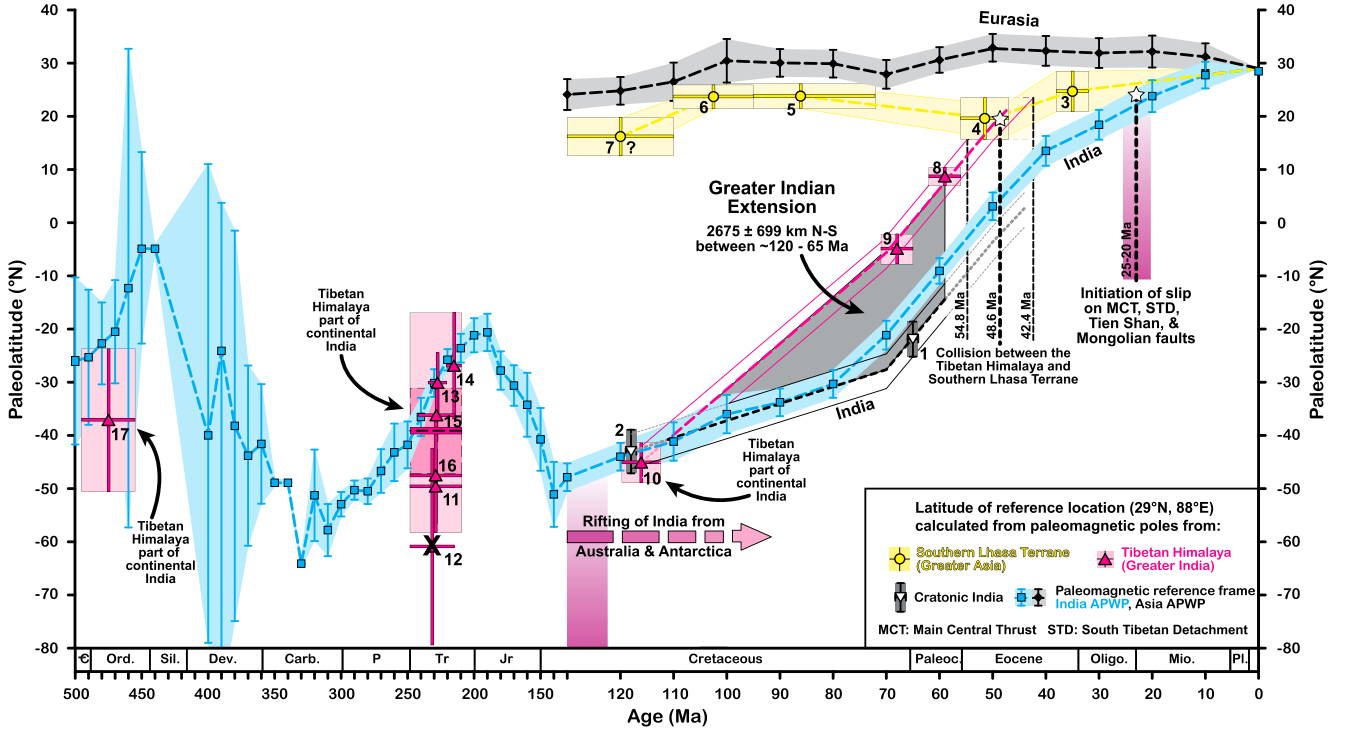


**Fig. S2.** Paleolatitudes of a reference site (29°N, 88°E) located on the present-day position of the Indus–Yarlung Suture Zone in Eurasian, Greater Asian, Tibetan Himalayan, and Indian reference frames. Numbers correspond to paleomagnetic poles described and listed in Table S1. Pl, Pliocene; Mio, Miocene; Oligo, Oligocene; Paleo., Paleocene; Jr, Jurassic; Tr, Triassic; P, Permian; Carb., Carboniferous; Dev., Devonian; Sil., Silurian; Ord, Ordovician; C, Cambrian; MCT, main central thrust; STD, South Tibetan detachment. Uncertainties in age are assigned based on the age of the units determined from either radiometric dates or geologic stages (17, 18), whereas latitude uncertainties are at the 95% confidence level. Question mark next to estimate 7 indicates that this pole may not fully average paleosecular variation.

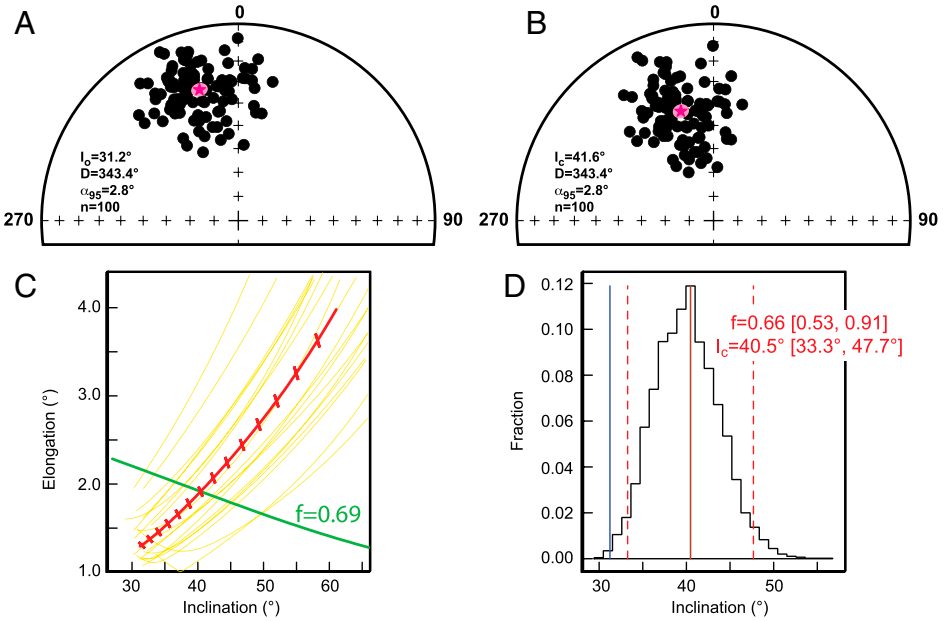


**Fig. S3.** E/I correction (15) of high-temperature, primary magnetic component of the Shexing formation redbeds at Maxiang, south, central Lhasa terrane (42). (*A*) Equal area plot of original paleomagnetic directions in tilt-corrected coordinates, with a mean inclination of 31.2° (magenta star, 95% confidence interval indicated in pink). Slight horizontal elongation of the direction distribution is consistent with sedimentary inclination shallowing. (*B*) E/I-corrected paleomagnetic directions after accounting for a flattening factor of 0.66. The E/I-corrected inclination is 41.6°. (*C*) Plot of elongation versus inclination for the TK03.geocentric axial dipole (GAD) paleosecular variation model (solid green line, ref. 15) and for the Shexing formation directions (barbed red line) for different flattening factors, *f*. Yellow lines are the results from 20 boot-strapped datasets. The crossing points of the Shexing formation and boot-strapped dataset with the TK03.GAD results represents the elongation/inclination pairs that are most consistent with the TK03. GAD field model. (*D*) Histogram of crossing points from 5,000 boot-strapped datasets. The most frequent flattening factor is $f = 0.66$, resulting in the distribution of directions shown in *B*.

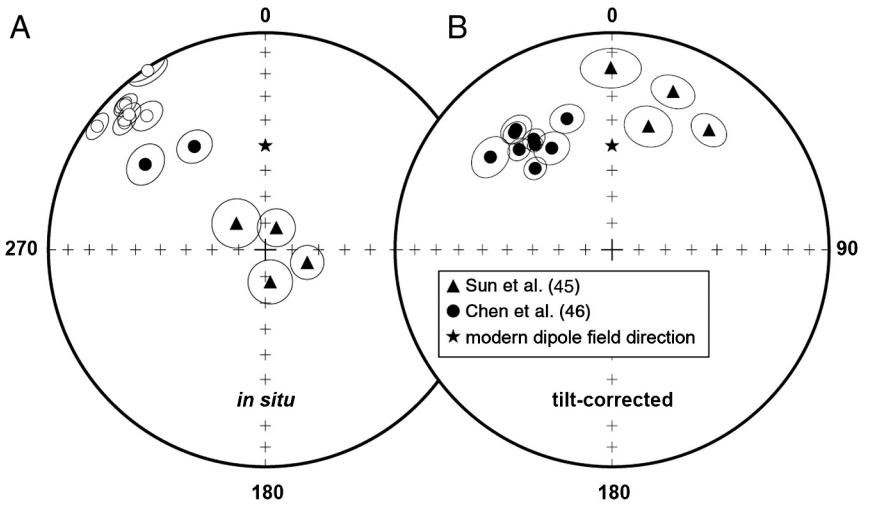


**Fig. S4.** Equal area plot of site mean directions from lower Cretaceous volcanic rocks from the central and western Lhasa terrane that pass our data quality criteria (45, 46). Downward (upward) pointing directions are shown as filled (open) symbols. Star indicates the present dipole magnetic field direction. Significant improvement in the clustering of inclinations from in situ coordinates (*A*) to tilt-corrected coordinates (*B*) is consistent with a prefolding magnetization. The noticeably different declination values observed in the two localities are consistent with differential vertical axis rotation because the emplacement of these lavas and justifies the use of latitude-only paleolatitude methods (*SI Text*).

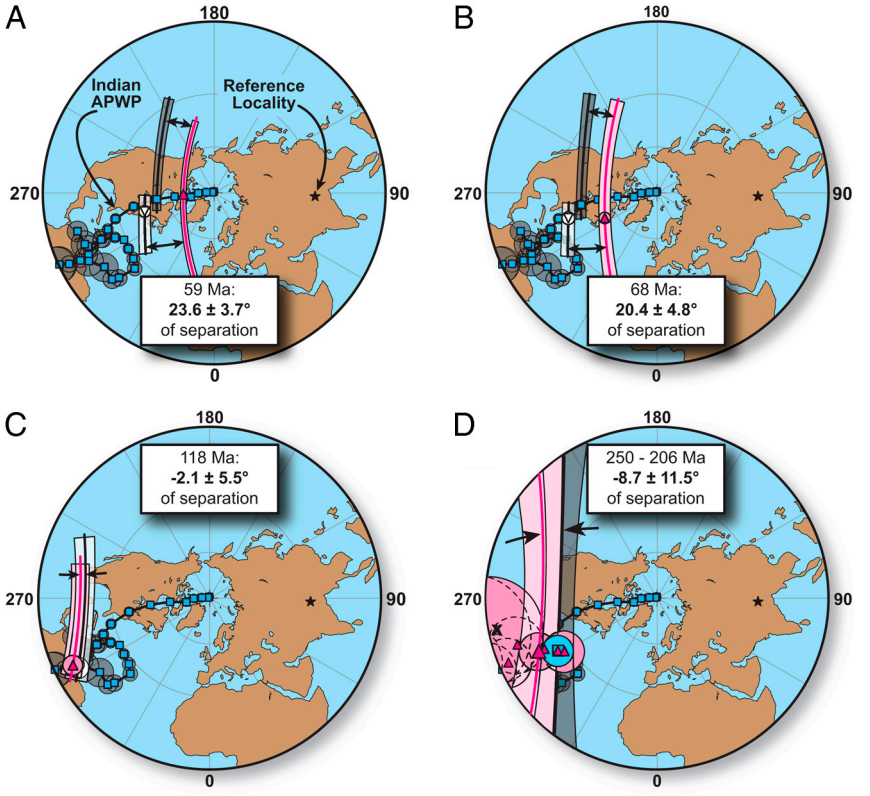


**Fig. S5.** Rotation-corrected paleomagnetic poles for the Tibetan Himalaya showing latitudinal separation between the Tibetan Himalaya and cratonic India for the (*A*) Paleocene, (*B*) latest Cretaceous, (*C*) early Cretaceous, and (*D*) Triassic. Ninety-five percent confidence limits of the pole positions are also shown.

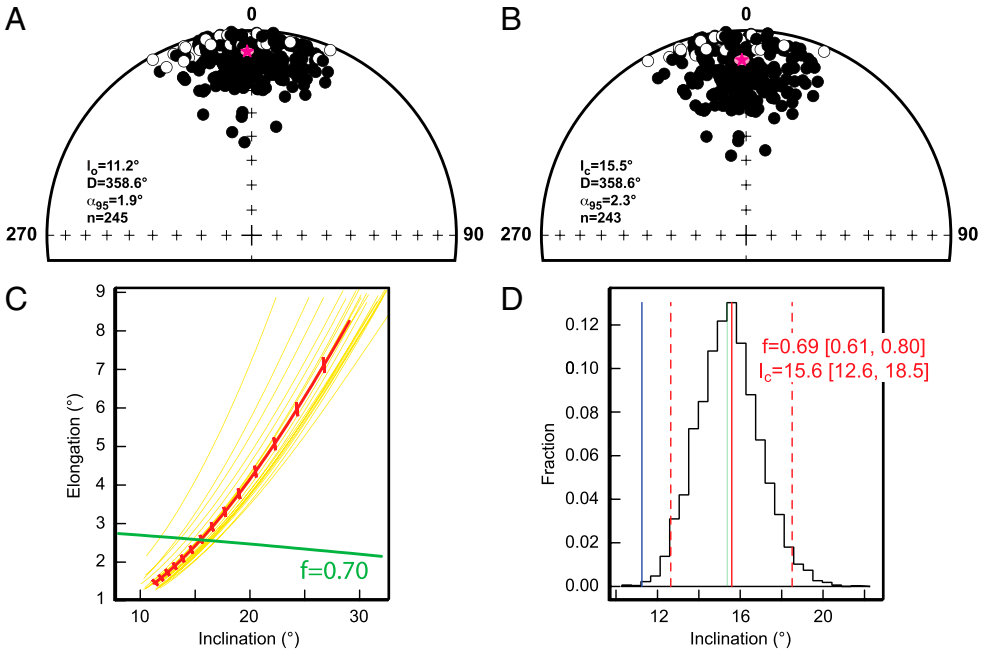


**Fig. S6.** E/I correction (15) of high-temperature, primary magnetic component of the Zongpu formation marine limestones at Gamba and Duela, southern Tibetan Himalaya (52, 59). Format of figures follows Figs. S3 and S4. (*A*) Distribution of 245 original paleomagnetic directions in tilt-corrected coordinates, with a mean inclination of 11.2°. Horizontal elongation of the direction distribution is consistent with sedimentary inclination shallowing. (*B*) E/I-corrected paleomagnetic directions after accounting for a flattening factor of 0.69 (*C* and *D*). The E/I-corrected inclination is 15.5°, indicating that inclination shallowing in these marine limestones is <5°.

## Other Supporting Information Files

Table S1 (DOC)
Table S2 (DOCX)
Table S3 (DOCX)
Table S4 (DOCX)
Table S5 (DOCX)
Table S6 (DOCX)
Table S7 (DOC)
Table S8 (DOCX)
Table S9 (DOCX)
Table S10 (DOCX)